Landslides (2021) 18:807–825
DOI 10.1007/s10346-020-01541-0
Received: 24 January 2020
Accepted: 16 September 2020
Published online: 6 October 2020

Dario Peduto · Mariantonia Santoro · Luigi Aceto · Luigi Borrelli · Giovanni Gullà

Full integration of geomorphological, geotechnical, A-DInSAR and damage data for detailed geometric-kinematic features of a slow-moving landslide in urban area

Abstract The reconnaissance, mapping and analysis of kinematic features of slow-moving landslides evolving along medium-deep sliding surfaces in urban areas can be a difficult task due to the presence and interactions of/with anthropic structures/infrastructures and human activities that can conceal morphological signs of landslide activity. The paper presents an integrated approach to investigate the boundaries, type of movement, kinematics and interactions (in terms of damage severity distribution) with the built environment of a roto-translational slow-moving landslide affecting the historic centre of Lungro town (Calabria region, southern Italy). For this purpose, ancillary multi-source data (e.g. geological-geomorphological features and geotechnical properties of geomaterials), both conventional inclinometer monitoring and innovative non-invasive remote sensing (i.e. A-DInSAR) displacement data were jointly analyzed and interpreted to derive the A-DInSAR-geotechnical velocity (DGV) map of the landslide. This result was then cross-compared with detailed information available on the visible effects (i.e. crack pattern and width) on the exposed buildings along with possible conditioning factors to displacement evolution (i.e. remedial works, sub-services, etc.). The full integration of multi-source data available at the slope scale, by maximizing each contribution, provided a comprehensive outline of kinematic-geometric landslide features that were used to investigate the damage distribution and to detect, if any, anomalous locations of damage severity and relative possible causes. This knowledge can be used to manage landslide risk in the short term and, in particular, is propaedeutic to set up an advanced coupled geotechnical-structural model to simulate both the landslide displacements and the behavior of interacting buildings and, therefore, to implement appropriate risk mitigation strategies over medium/long period.

Keywords Slow-moving landslides · Geotechnical data · Monitoring · Damage · A-DInSAR

Introduction

Studies and investigations pursuing the characterization of landslides represent the necessary background to identify the triggering factors and the possible causes within risk assessment activities aimed at predicting and mitigating the associated consequences. The in-depth knowledge of geometric-kinematic features, corroborated by the analysis of the behaviour of the exposed elements interacting with the landslide mechanism, can help in developing, when necessary, more sophisticated numerical analyses given that the mechanical soil properties and the groundwater regimen are adequately defined (Cascini et al. 2006; Cotecchia et al. 2016; Merodo et al. 2014). As for slow-moving landslides evolving along medium/deep slip surfaces in urban areas, the detection, mapping and analysis of kinematics may be often hampered by the presence of anthropic structures (e.g. buildings or any kind of facility) and infrastructures (e.g. road network, bridges) and human activities (Gullà et al. 2017; Peduto et al. 2016, 2018b). Urbanization, indeed, can limit or make it difficult the recognisance of geomorphological features (via both conventional image interpretation and in situ surveys) that usually help in landslide mapping (Guzzetti et al. 2012; Antronico et al. 2015; Jaboyedoff et al. 2019). Furthermore, both topographic and geotechnical monitoring equipment is not easy to be installed when the landslide-affected area is densely built up (Gullà et al. 2017). Conversely, it is exactly the presence of the exposed elements that identifies the unstable slopes as at risk areas (Borrelli and Gullà 2017; Fell et al. 2008; Corominas et al. 2014; Cigna et al. 2014; Ferlisi et al. 2019; Peduto et al. 2019b; Winter et al. 2016). Therein, more sophisticated numerical analysis can be developed—if soil mechanical properties and the groundwater regimen are adequately defined—for appropriate hazard and vulnerability assessment, which is necessary to plan and design reliable control works and risk mitigation strategies.

In such contexts, several scientific papers proved the effectiveness of multi-sensor monitoring plans. These latter rely on the combination of conventional and innovative technologies to overcome the limits of a single technique (Abolmasov et al. 2015; Antronico et al. 2015; Bianchini et al. 2014; Casagli et al. 2017; Calò et al. 2014; Di Maio et al. 2018; Frattini et al. 2018; Gullà et al. 2017; Peduto et al. 2016; Nappo et al. 2019; Wasowski and Pisano 2019). Among recent techniques, the processing of synthetic aperture radar images via advanced differential interferometric techniques (A-DInSAR) is a well-established non-invasive cost-effective option for surface displacement monitoring of natural/anthropogenic benchmarks (persistent scatterers) even over large areas with mm/year accuracy (Nicodemo et al. 2017a; Peduto et al. 2018a, 2019a) and precision (Crosetto et al. 2016; Hanssen 2001; Wasowski and Bovenga 2014) on the velocity and sub-centimetre accuracy of the single displacement measurement (Herrera et al. 2009; Peduto et al. 2017a;). Indeed, many authors showed that these data can be helpful in detecting, mapping and defining the state of activity of (very to extremely, according to Cruden and Varnes 1996) slow-moving landslides (Cascini et al. 2009, 2010; Cigna et al. 2014; Colesanti and Wasowski 2006; Crosetto et al. 2013, 2018; Frattini et al. 2018; Gullà et al. 2017; Auflič et al. 2018; Lu et al. 2014, Raspini et al. 2017, 2018; Tofani et al. 2013; Wasowski and Bovenga 2014). Most of these works were carried out at basin and municipal scales with very few examples referred to the single slope scale (Castaldo et al. 2015; Frattini et al. 2018; Herrera et al. 2013; Hilley et al. 2004; Peduto et al. 2016; Wasowski and Pisano 2019). More recently, the contribution of A-DInSAR data was demonstrated also for what concerns the analysis of the behaviour

of structures (Bianchini et al. 2015; Cascini et al. 2013; Del Soldato et al. 2019; Frattini et al. 2013; Nicodemo et al. 2018; Peduto et al. 2016, 2017a, b, 2019b) and infrastructure (Infante et al. 2018; Nappo et al. 2019; North et al. 2017; Wasowski et al. 2017) interacting with slow-moving landslide mechanisms. As for the role played by the exposed elements in the analysis of built-up unstable slopes, buildings, roads, bridges and any kind of man-made structure can play as movement indicators (Borrelli et al. 2018; Cascini et al. 2013; Di Maio et al. 2018; Ciampalini et al. 2014; Palmisano et al. 2016). Therefore, they can contribute to outline the evolutionary model of a given landslide and, more in general, its geometric and kinematic features.

A further contribution to the use of multi-sensor multi-source data for landslide characterization is provided by the present work with reference to the slope scale. For this purpose, a procedure that combines geological-geomorphological features, ancillary data (i.e. characteristics of geomaterials, landslide inventory), conventional geotechnical monitoring (i.e. inclinometer measures referred to the geomaterials), A-DInSAR data and the results of damage surveys, also taking into account the presence of possible anthropic conditioning factors on the slope stability, is proposed. The procedure is tested with reference to the historic centre of Lungro (Calabria region, southern Italy), which has been severely affected by very slow to slow-moving (Cruden and Varnes 1996) landslides for many years, as highlighted by both conventional and innovative monitoring data available since early 2000s (Guerricchio et al. 2012; Gullà et al. 2017; Peduto et al. 2017b, 2018b).

The present study takes advantage of previous researches carried out at the municipal scale in Lungro area and, starting from the full integration of the above-mentioned data available at the slope scale, by maximizing each contribution, provides a comprehensive outline of kinematic-geometric landslide features that are used to investigate the distribution of damage to buildings in the affected area. An original product of the present work is the *A-DInSAR-Geotechnical velocity (DGV)* map that, starting from a joint analysis of inclinometer measurements and A-DInSAR data (examples in literature are provided by Tofani et al. 2013; Calò et al. 2014; Del Soldato et al. 2018; Wasowski and Pisano 2019), carries out a novel quantitative comparison allowing for the assessment of the prevailing local velocity versus/direction and the related projected modulus that are jointly represented as easy-to-read velocity vectors (at the ground surface) over the landslide-affected area. The followed approach helps in distinguishing those portions of the landslide that exhibit either mainly rotational or translational displacements. Furthermore, the quantitative information provided by the projected velocity values is synergistically analyzed with respect to the severity and distribution of the damage recorded to buildings located in different portions of the analyzed landslide. Finally, a few detected locations with anomalous damage severity level are investigated taking into account possible additional conditioning factors of the building performance associated with the presence of buried sub-services whose interaction with landslide mechanism is not yet adequately proved.

The gathered insight into kinematics, the geometric features and associated (anomalous) damage severity distribution within the landslide-affected area represent the necessary background for the definition of subsequent coupled geotechnical-structural models useful for sophisticate quantitative analyses aimed at managing the landslide risk over medium/long period under sustainable social-economic conditions.

Materials

Geology and geomorphology: urban area and historic centre

The north-western portion of the study area presents the Lungro-Verbicaro Unit (Fig. 1), consisting of metapelites and metacarbonates (Iannace et al. 2005; Antronico et al. 2015). Close to the urban area, the upper portion of the Diamante-Terranova Unit (Lower Jurassic-Cretaceous), made up of phyllites and slates, crops out. Both lithotypes form a "melange structure" made up of blocks and fragments of different nature (e.g. phyllites, slates and metacarbonates) in a prevalently clayey matrix, originating from phyllites degradation (Antronico et al. 2013, 2015). An Upper Tortonian–Messinian sequence composed by coarse sandstone and shale interbedded with gypsiferous sandstone and gypsum overlays the Diamante-Terranova Unit metasediments. The Early Miocene succession then ends with deposits dating back to the Middle Pliocene-Pleistocene, represented by sandy and conglomeratic beds. Colluvium and landslide debris covers, with a maximum thickness of approximately 10 meters, mantle the phyllite bedrock on the slopes (Fig. 1) (Antronico et al. 2013; Gullà et al. 2017; Peduto et al. 2016). Using multi-temporal aerial photographs dated 1955 (at 1:33,000 scale), 1980 (at 1:25,000 scale), 1991 (at 1:33,000 scale) and 2001 (at 1:15,000 scale), and field surveys, previous studies provided the landslide inventory map of the study area (Antronico et al. 2013; Gullà et al. 2017; Peduto et al. 2016) (Fig. 1). The area is affected by a number of landslides of various types that were classified according to Varnes (1978). Subsequently, Gullà et al. (2017) based on some of the elements that concur in defining the landslide geotechnical model (i.e. the depth of the slip surface, the width and the length of the landslide body, the involved geomaterials and the landslide type) proposed four landslide groups ("typified" landslides, hereafter) as shown in Fig. 1. In particular, category A landslides, whose type can be ascribed to complex (slide-flow) landslides, are shallower than 10 m and affect detrital-colluvial covers; category B landslides, extending to depths between 10 and 20 m, affect deeply weathered and chaotic phyllites and belong to the complex (slide-flow) landslide type; category C landslides, extending to depths between 20 and 30 m, affect deeply weathered and chaotic phyllites and belong to the so called landslide zone (Antronico et al. 2013), representing an area where clustering of mass movements is so tight that it is difficult to distinguish the different bodies (mainly including landslides of the slide-flow type according to Sorriso-Valvo and Sylvester 1993; Antronico et al. 1996; Greco et al. 2007); and category D landslides, extending to depths between 20 and 30 m, affect weathered and chaotic phyllites and belong to the slide type. A summary is shown in Table 1 (modified from Gullà et al. 2017).

Geomorphological and geotechnical landslide features

The present study focuses on the Lungro historic centre, where, based on geological-geomorphological criteria and monitoring data, previous studies (e.g. Antronico et al. 2013, 2015; Peduto et al. 2016; Gullà et al. 2017) distinguished and mapped an active, medium-deep and slow-moving landslide of slide type, typified as T_D (Fig. 1 and Table 1). Starting from the literature data, a new mapping of this landslide was produced (Fig. 2a).

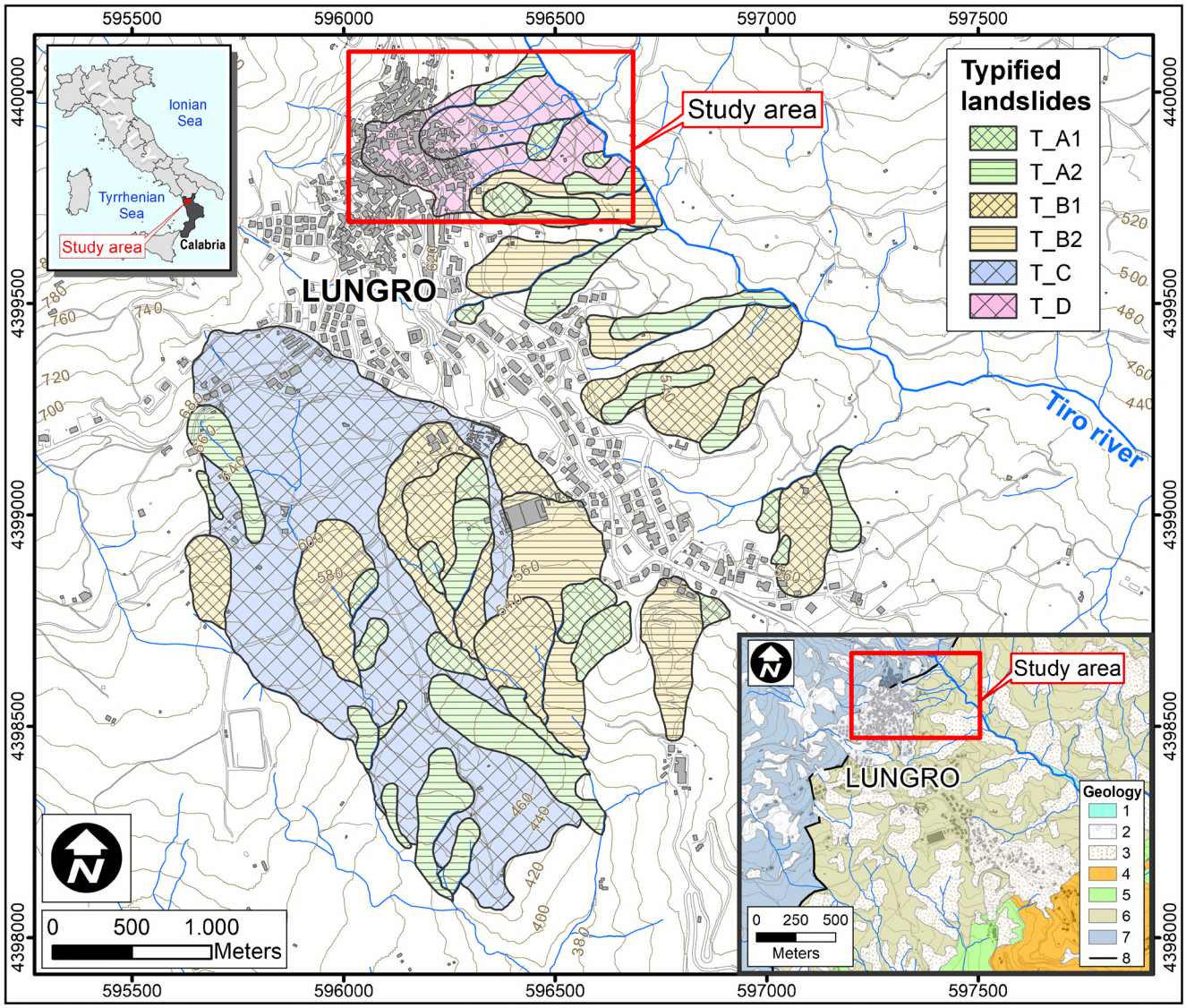

Fig. 1 Geological and Geomorphological classification of landslides: (1) Alluvian Deposits (Holocene); (2) Detritical Carbonate Deposists (Holocene); (3) Detritical-Colluvial Cover (Holocene); (4) Middle Pliocene-Pleistocene Succession; (5) Middle Tortorian-Messinian Succession; (6) Diamante-Terranova Unit (Lower Jurassic-Cretaceous); (7) Lungro-Verbicaro Unit (Anisian-Lower Burdigalian); (8) Tectonic contact. For the typified landslide categories the reader can refer to Table 1 (modified from Gullà et al. 2017 and Peduto et al. 2016)

Table 1 Typified landslides

Typified landslide	Width [m]	Length [m]	Depth [m]	Involved soil	Kinematic type
T_A1	25–100	≤ 180	About 6	Detritic-colluvial covers (COV)	Complex landslide
T_A2	15–100	≥ 80	About 10		
T_B1	90–260	130–550	10–20	Deeply weathered and chaotic phyllites (CHAOT)	Complex landslide
T_B2	80–220	> 300	10–16		
T_C	830	1500	20–30	Deeply weathered and chaotic phyllites (CHAOT)	Landslide zone
T_D	100–250	350–550	20–30/10–15	Weathered and chaotic phyllites (CHAOT)	Slide

COV stands for Cover and CHAOT stands for Chaotic (see description in section *Geology and geomorphology: urban area and historic centre*) (modified from Gullà et al. 2017)

The landslide upgrade was performed, following geomorphological criteria proposed by Cruden and Varnes (1996), through interpretation of traditional aerial photographs, Google Earth satellite images, coupled with analyses of a high-resolution DTM (i.e. DTM with 1-m ground resolution, deriving from LiDAR scanning on an aerial platform acquired during 2012 by the Italian Ministry for the Environment, Land and Sea), and detailed multi-temporal field surveys.

The landslide involves large part of Lungro historic centre, where most buildings are located (Fig. 2a). It extends over an area of about 7 ha and occurs on a slope gradient of about 15°. The landslide, which is about 440 m long and 180 m wide, ranges from an elevation of 594 m (in the upper part of the slope) down to 488 m (at the valley bottom). Two distinct bodies (Fig. 2a) form the landslide: a western active landslide body (~ 1.3 ha) and an eastern active body (~ 5.3 ha), which overlaps with the previous one. The landslide has a crown with an irregular shape (400 m long), and the main scarp is not evident; the eastern body shows a semi-circular minor scarp with smoothed and eroded morphology. The right and left flanks (the latter one well defined) are similarly incised and sub-rectilinear in shape with nearly straight traces and coincide with two ephemeral stream channels that drain water towards the Tiro River. Two active secondary landslides typified by Gullà et al. (2017) as T_A1 and T_A2 mask these flanks, in their terminal sector (Fig. 2a). In this area, the emergent toe of the failure surface was only locally found (Fig. 2a). Here, some temporary springs, characterized by an aligned drainage pattern whose flow rate increases during the rainfall period, have been observed.

The observed geomorphological features of the landslide indicate that the two bodies can be classified as translational landslides with minor rotational components. Particularly, the landslide motions are mainly translational, with slight rotational character immediately downstream of the two escarpment sectors.

As for the involved geomaterials, the six available geotechnical boreholes, equipped with inclinometers, allow recognizing the geomaterials that characterize the stratigraphic sequence of the landslide site (Fig. 2b). At the top of the stratigraphic sequence, it is observed 12–24 m of colluvial and detrital soils (named COV) and then 22–68 m of soils from degraded phyllites (named CHAOT). Along the S01 borehole, at 40 m below the ground surface, it is observed the presence of carbonate rocks (i.e. dolostones and limestones).

In addition, all inclinometer data show well-defined sliding surface positions (Fig. 2b) of which the deepest ones are located approximately 18–27 m below ground surface. Inclinometers S19 and S20 show a second sliding surface approximately 10–15 m deep (Fig. 2b).

The longitudinal section of Fig. 2c shows that the landslide mass moves along a low angle (i.e. approximately 15°) mainly translational surface almost parallel to the ground surface. The total volume of the failed material is about 2 million cubic meters.

The COV and CHAOT geomaterials that are involved in landslide movements have similar grain size distributions (Fig. 3a). In particular, the COV geomaterial has a variable particle size ranging from sandy silty gravel to sandy gravelly silt with clay; for the CHAOT geomaterial, the grain size varies from sandy silty gravel to sandy silt with clay. Although the COV and CHAOT geomaterials present wide grain size variability, we can observe in Fig. 3a a significant presence of grain size distribution curves with a cumulative percentage of clay and silt greater than about 50%, pertaining to samples taken at depths varying from about 5 to 35 m below ground surface. In particular, the finer samples are prevalently located from 15 to 25 m below ground surface; within this latter depth range, the inclinometer measurements identify the positions of the sliding surfaces as shown in Fig. 2b by the available geotechnical logs. This issue indicates, as expected, that the sliding surfaces develop where the COV or CHAOT geomaterials present grain size fractions mainly consisting of clay and silt.

The COV and CHAOT similarity and their general heterogeneity are confirmed by the distribution of the test points in the activity-plasticity charts (Fig. 3b). In particular, the finer fraction of COV geomaterial is classifiable as prevalently inorganic clays with medium-low plasticity; the finer fraction of CHAOT geomaterial is an inorganic clays with medium-low plasticity. In Fig. 3c, some index properties are shown. In particular, for the volume of geomaterials involved in the landslide bodies (i.e. COV and CHAOT geomaterials above the sliding surfaces), the representative values of the natural and saturated unit weight can be assumed 22 kN/m^3 and 24 kN/m^3 with reference to the average values of all COV- and CHAOT-tested samples (Fig. 3c).

Geotechnical and remote sensing displacement monitoring

Within Lungro historic centre, deep ground displacement measurements were performed using a network of six inclinometers (Gullà et al. 2017), Fig. 2. Measurements were carried out from April 2006 until May 2014. The measured cumulative deep displacement moduli are generally constant with depth, and show sharp and well-defined slip surfaces (Fig. 2b). Figure 4 shows the velocity values of inclinometer measurements along with their azimuthal directions with reference to the period September 2006 to March 2010 (Fig. 4a) and October 2011 to May 2014 (Fig. 4b) as recorded within the landslide body.

A-DInSAR data available for Lungro historic centre were processed according to the SAR tomographic analysis (Fornaro et al. 2009, 2014). The A-DInSAR dataset, whose spatial velocity distribution along the Line of Sight (LOS) sensor-target direction is shown in Fig. 4, consists of 35 ENVISAT images acquired on ascending orbit (from August 2003 to February 2010; see Fig. 4a) as well as 39 Cosmo-SkyMed (CSK) images acquired on ascending orbit (from October 2012 to April 2014; see Fig. 4b). In Figs. 4a and b, velocity values measured by inclinometers and A-DInSAR data are shown with reference to the overlap periods.

Damage to buildings

The buildings in the analyzed portion of Lungro historic centre belong to a rather homogeneous urban fabric composed by masonry low-rise structures (i.e. 2–3 floors), mainly made of disorganized stones (pebbles, or erratic/irregular stones), on shallow foundations with ages ranging from 70 to 300 years (Nicodemo et al. 2020; Peduto et al. 2017b).

As for the damage, the available dataset resulted from a survey carried out in October 2015 over the entire urban area (Peduto et al. 2017b, 2018b). In particular, building damage fact-sheets (Ferlisi et al. 2015; Nicodemo et al. 2017a) were filled in and the damage severity levels of the surveyed buildings were classified according to Burland et al. (1977). In particular, five classes (Do = negligible, D1 = very slight, D2 = slight; D3 = moderate; D4 =

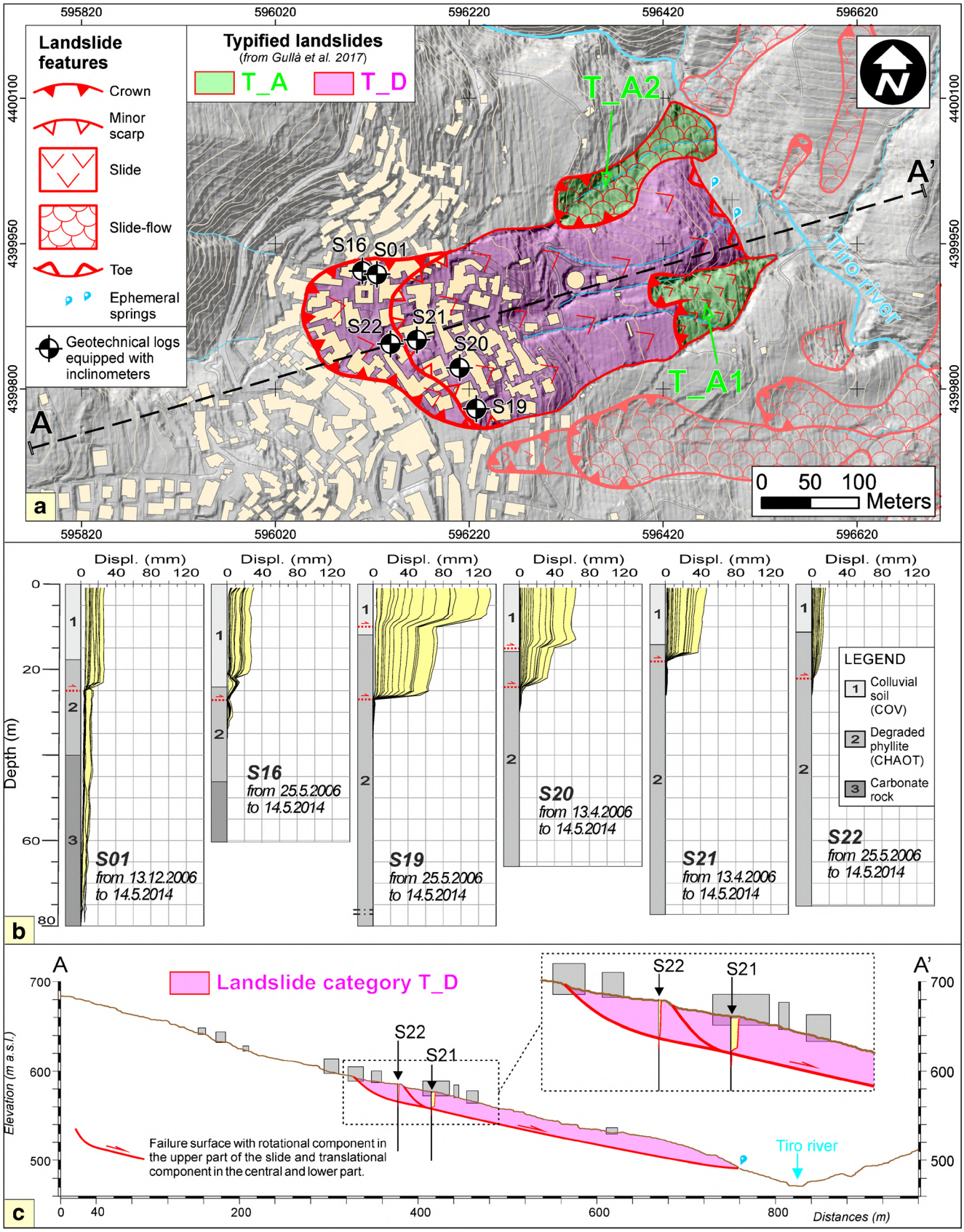

Fig. 2 **a** Landslide map with localization of geotechnical logs and inclinometers. **b** Geotechnical logs and inclinometer measurements from 2006 to 2014. **c** Cross-section of the landslide

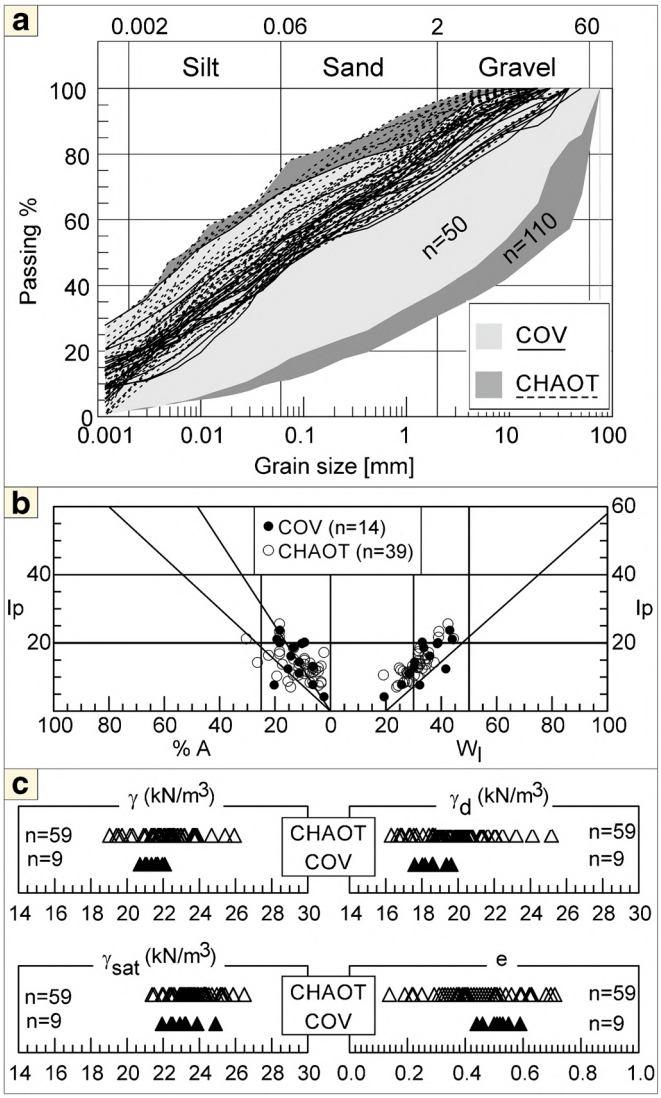

Fig. 3 Geotechnical properties of geomaterials. **a** Grain size distribution curve of the colluvial soils (COV) and degraded phyllites (CHAOT). **b** Activity chart and Casagrande Plasticity chart. **c** Natural, dry and saturated unit weight and porosity index of COV and CHAOT geomaterials

severe; D5 = very severe) were identified that, based on the width of cracks on building facades and their distribution as well as the easy of repair, mainly reflect the attainment of damage affecting the building aesthetics (D1–D2), causing a loss of functionality (D3) or even compromising their stability (D4–D5). Figure 5 shows the damage distribution and some pictures of damaged buildings within the landslide affecting Lungro historic centre.

Method

The followed procedure consists of two phases pursuing respectively: (i) the retrieval of both geometric and kinematic features from multi-source monitoring data and information on related effects (i.e. damage) on buildings and (ii) a synoptic analysis of all available data aimed at pointing out the factors conditioning the evolution and the interaction with the exposed elements (Fig. 6).

Phase I is twofold. In *Phase Ia*, the landslide map, inclinometric data and A-DInSAR data are used to validate the kinematic model of the landslide defined on geological-geomorphological basis. Then, A-DInSAR and inclinometric data are fully integrated to derive the *A-DInSAR-Geotechnical Velocity (DGV) map*, which provides 3D velocity vectors (with assigned moduli, direction and versus) of the landslide based on the joint analysis of landslide boundaries and slip surfaces derived from geomorphological criteria and inclinometers together with information on the digital elevation model (DEM), the orbit and the acquisition geometry of DInSAR data. In particular, the direction of the 3D velocity vector and its angles in the horizontal and vertical plane are described by the three types shown in Fig. 7 (Type I, Type IIa, Type IIb, hereafter). The background idea is that inclinometer and A-DInSAR data (constrained by their respective 1D measurement directions, i.e. horizontal along the azimuth for inclinometers and along the LOS for A-DInSAR), if properly combined, can help in reconstructing the "real" velocity vector of the landslide. This is of key importance when quantitative analyses concerning both the kinematics and related effects on structures/infrastructures are to be performed. In previous works carried out at the basin scale (Bianchini et al. 2012; Cascini et al. 2010), projections of A-DInSAR data from the LOS to the steepest slope

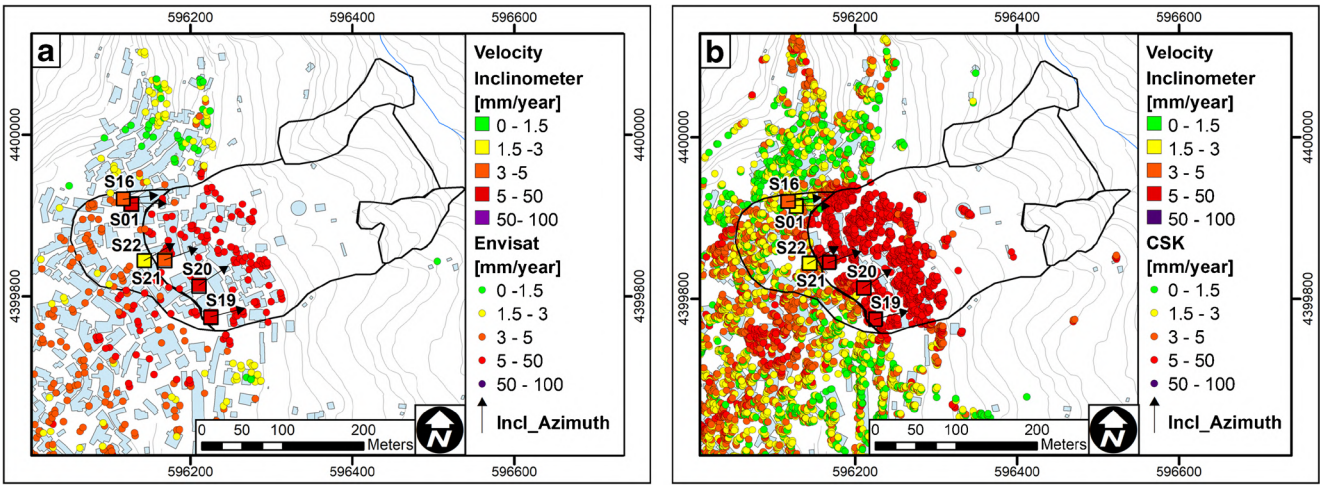

Fig. 4 Geotechnical and remote sensing velocity monitoring in Lungro historic centre represented during the overlap periods: (a) inclinometers (September 2006–March 2010) and Envisat (September 2006–February 2010) data; (b) inclinometers (October 2011–May 2014) and Cosmo-SkyMed data (October 2012–April 2014). A-DInSAR velocity is provided along the line of sight (LOS) direction. The black arrows indicate the azimuthal direction of the inclinometer measurement

direction were adopted; in this study, a procedure at the scale of the single slope is proposed to accomplish the full integration of A-DInSAR and inclinometer data to reconstruct roto-translational displacements. In particular, firstly, A-DInSAR data and the available inclinometric

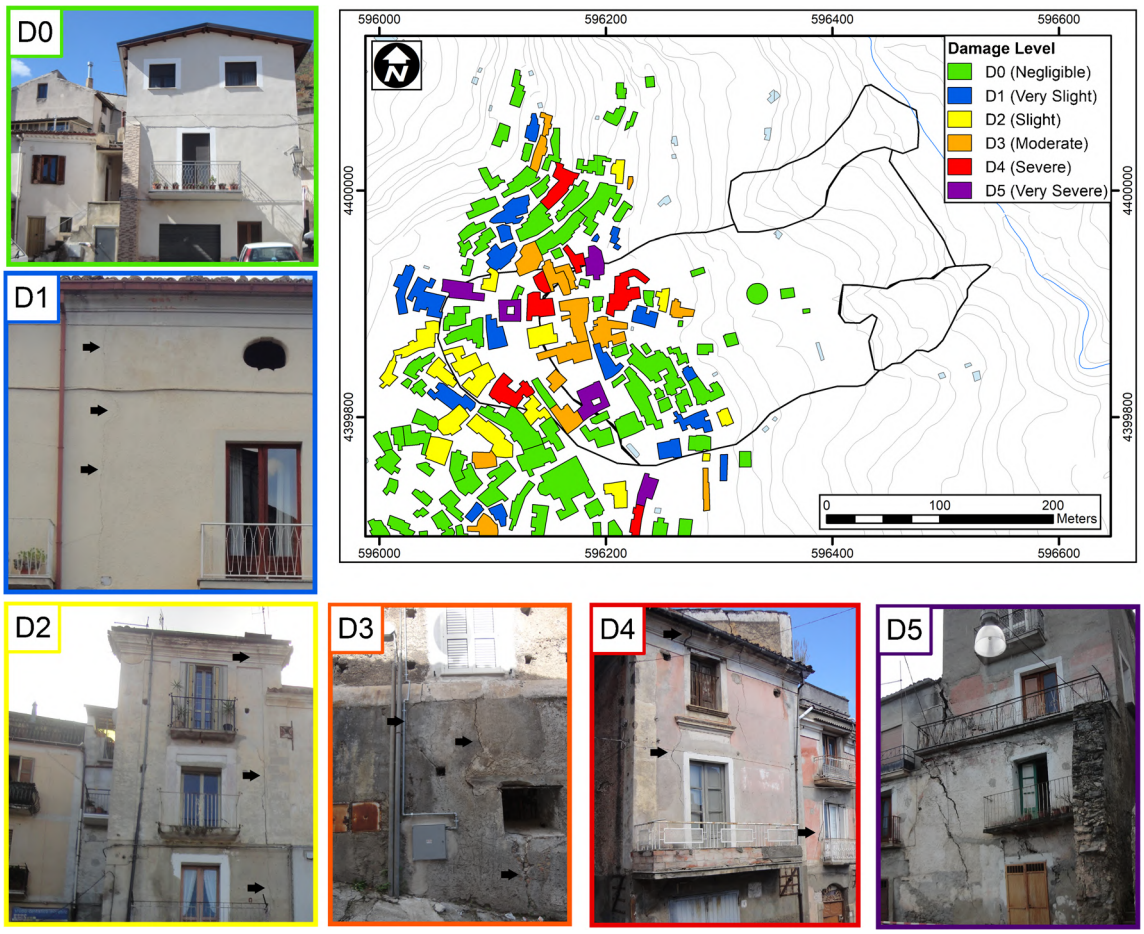

Fig. 5 Distribution and severity level of damage to masonry buildings in the historic centre of Lungro (modified from Peduto et al. 2018b)

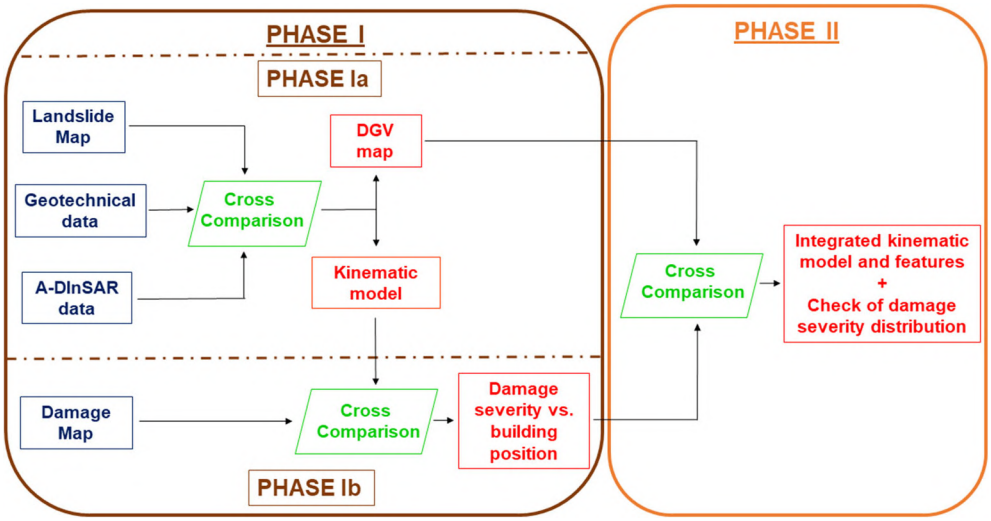

Fig. 6 Framework of the procedure

measurements (relevant to the most superficial measurement carried out at 1-m depth) are projected along the same directions, which are identified as the ones pertaining to the specific portion of the landslide where both measurement points are located (see Fig. 7). Then, the representative velocity direction is defined as the direction providing the best cross-fitting in terms of (minimum) ΔV between the projected A-DInSAR and inclinometer velocity moduli. To this aim (see Fig. 7), adapting the procedure proposed by Cascini et al. (2010, 2013), the representative velocity vector has an inclination with respect to the vertical plane equal to the angle of either the steepest slope direction (β) or the sliding surface (in some cases considering either the lower (γ_1) or the upper (γ_2) slip surface should both of them be detected along the inclinometer vertical). As for the reference direction on the horizontal axis (α), it is assumed as either the inclinometer azimuth direction or the aspect slope angle derived from the digital elevation model (DEM). This allows defining three different types of projections. When both inclinometer and PSs are located within the landslide body (where the translation movement is assumed to prevail), both measurements are projected along the steepest slope direction (Type I in Fig. 7) with the aspect (α, in the horizontal plane) and the slope (β, in the vertical plane) angles both derived from the DEM. Then, for measurement points (i.e. inclinometers and PSs) both located in the head of the landslide—where the rotational movements prevail—measurements follow Type II (Fig. 7) projection for which α (the angle in the horizontal plane) is assumed equal to the azimuth angle of the inclinometer and γ represents the inclination angle (in the vertical plane) of the sliding surface. In this latter case, where the inclinometer shows the presence of two sliding surfaces, two angles are considered (i.e. γ_1 or γ_2) representing the inclination angles (in the vertical plane) of the lower or upper sliding surface respectively. In particular, in case of projections along the lower sliding surface (see Fig. 7) the landslide movement is mainly translational evolving along a sliding surface sub-parallel to the ground surface; thus, the angle γ_1 is approximated to the slope angle derived from the DEM. Instead, in case of projections along the upper slip surface, the rotational component prevails and the γ_2 angle is equal to the inclination angle of the upper sliding surface detected by the inclinometer (Fig. 7). It is noteworthy that, for the case study at hand, the above assumptions are cross-checked and the projection type providing the best fitting between A-DInSAR and inclinometric measurements within different portions of the landslide is finally adopted to project each A-DInSAR LOS velocity to the representative velocity directions represented in the *DGV map*. Furthermore, taking into account that the projection

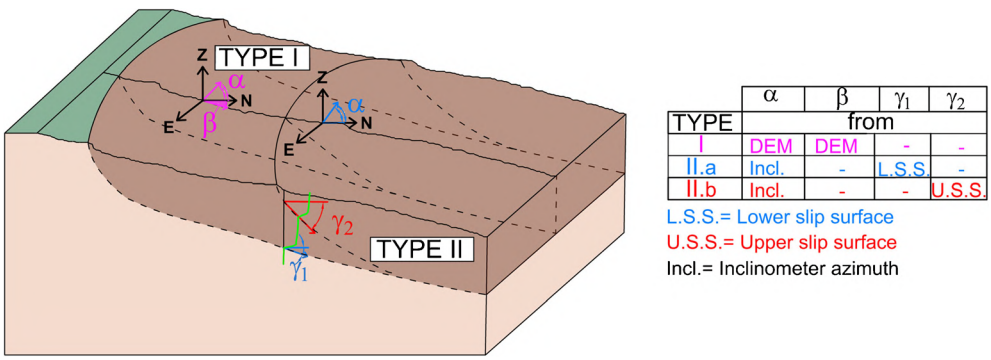

TYPE	α	β	γ1	γ2
	from			
I	DEM	DEM	-	-
II.a	Incl.	-	L.S.S.	-
II.b	Incl.	-	-	U.S.S.

L.S.S.= Lower slip surface
U.S.S.= Upper slip surface
Incl.= Inclinometer azimuth

Fig. 7 Sketch of the conceptual models (kinematic types) used for A-DInSAR data projection based on the inclinometer data, the digital elevation model and the position of the PS with respect to the cross-section of the landslide

operations of A-DInSAR data from the LOS to the representative direction can be biased by errors (see for instance Cascini et al. 2010; Colesanti and Wasowski 2006; Wasowski and Pisano 2019) related to the sensitivity of SAR sensor acquisition geometry with respect to the topography (slope and aspect angles) as well as to the movement direction provided by the azimuth inclinometer (Wasowski and Pisano 2019), A-DInSAR projected velocity vectors considered in the DGV map are selected among those for which the projection coefficient from the V_{LOS} modulus to the representative direction are below the threshold value of 3.33, as proposed in literature by some authors (Cascini et al. 2013; Herrera et al. 2013; Plank et al. 2010).

In *Phase Ib*, the map of damaged buildings is compared with the kinematic model of the landslide. In particular, the distribution of damage severity level is analyzed with respect to the position of the building within the landslide-affected area. Indeed, the performance of the exposed building (Palmisano et al. 2016) or infrastructure (Nappo et al. 2019) on the unstable slope is influenced by its position in the landslide area and its kinematic model as well as by the interaction between the building foundations and the unstable soil volumes.

In *Phase II*, the consistency of the *A-DInSAR-geotechnical velocity (DGV)* map (resulting from Phase Ia) and the distribution of building damage severity (resulting from Phase Ib) is cross-checked also addressing further investigations aimed at deepening observed discrepancies, if any.

Results

Phase Ia: Kinematic model and A-DInSAR-geotechnical velocity (DGV) map

As a first step, the integrated analysis of the landslide geomorphological features, geotechnical logs and inclinometer data allowed to confirm the kinematic model of the landslide based on geomorphological data. In particular, the longitudinal cross-section shown in Fig. 2c highlights that the landslide mass moves along a low angle, roughly translational surface (at depths ranging from 18 up to approximately 27 m) with little rotational component. Particularly, the sliding surface develops with a mainly translational component in the central and lower sector of the landslide and with slight rotational components in its upper sector immediately downstream of the two escarpments. In the lowermost sector of the landslide, the slip surface exhibits a rising toe segment.

As a second step, Envisat and Cosmo-SkyMed data were compared with six available inclinometer measurements (Figs. 2 and 8). For this purpose, assuming that the landslide movement is homogeneous in areas close to the inclinometers, each inclinometer was associated with the PSs falling within a circular buffer of 20 m.

Subsequently, for each inclinometer and the associated PSs, displacement data were projected according to both TYPE I or TYPE II (see Fig. 7) in order to find out which projection provided the best fitting (Fig. 9). For sake of simplicity, Fig. 9 shows the results only for inclinometers S19 and S20. For these two inclinometers detecting two sliding surfaces (Fig. 2b), having assumed that the PSs move in the same way as the closest inclinometer, the angle in the horizontal plane (α) was assumed equal to the azimuth of the inclinometer; whereas the angle in vertical plane was assumed equal to either the ground slope angle (β) or the inclination angles of the upper (γ_2)/lower (γ_1) sliding surface.

Then, a quantitative comparison among possible projections for all the inclinometers and the PSs included in the surrounding 20-m buffer was performed. In particular, ΔV, which is the difference between the average annual velocity of the inclinometer and the average A-DInSAR annual velocity projected either along the steepest slope direction or the lower/upper slip surfaces of those PSs included in the 20-m buffer, was computed. The results for both Envisat and Cosmo-SkyMed data are synthesized in Table 2 showing that the best fitting projection changes according to the position of the inclinometer in the landslide body. Indeed, it seems that when the inclinometer crosses only the lower sliding surface (S01, S16, S21, S22), the projection operations provide very similar results either along the (lower) sliding surface or the steepest slope direction (on the ground surface). This could be justified by the prevailing translational mechanism with a sliding surface sub-parallel to the ground surface in this portion of the landslide body, as it also resulted from the geomorphological analysis and was validated by the kinematic model.

As for S19-S20 inclinometers (see Fig. 9), two (lower and upper) slip surfaces are distinguished (see Figs. 2b and 8) because they intersect the head of the eastern secondary landslide body and the main body of the landslide. In these cases, the projection along the upper/lower sliding surfaces seems to provide the best fitting (see Fig. 9 and Table 2) revealing, in this portion of the landslide, the effects of subvertical displacement associated with the rotational component that also the geomorphological analysis pointed out.

Therefore, based on the above considerations, the *DGV maps* within the Lungro historic centre were derived by including all A-DInSAR data within both the landslide perimeter and a 30-m buffer around the landslide boundaries to consider the errors related to landslide mapping and the localization of PSs as well. The three *kinematic types* shown in Fig. 7 were considered. Accordingly, the velocity values of PSs located on the main body of the landslide were projected along the steepest slope direction (see Table 2) considering both α and β angles deriving from the DEM (Type I). As for PSs positioned near either the landslide head/crown or an inclinometer, the velocity values were projected assuming the angle (α) in the horizontal plane equal to the inclinometer azimuth and the angle in the vertical plane equal to the inclination of the lower (γ_1 according to TYPE IIa) or upper slip surface (γ_2 according to Type IIb) in agreement with the results of the best fitting shown in Table 2.

By implementing the kinematic types for both datasets, two vector maps were derived (Fig. 10a and b). Then, the point-wise A-DInSAR velocity data were interpolated via IDW method in GIS environment using a grid cell of 2 × 2 m for CSK and 10×10 m for Envisat to account for different average sensor ground resolution (i.e. ~ 6 × 24 m, respectively, in azimuth and range for Envisat and 3 × 3 m for CSK, Wasowski and Bovenga 2014, Peduto et al. 2015).

The *DGV maps* (Fig. 10c and d) exhibit comparable velocity values during both periods (i.e. 2003–2010 and 2012–2014). In particular, both Envisat and Cosmo-SkyMed velocity maps show a non-homogeneous distribution of velocities inside the landslide with higher velocity values concentrating at the head, along the boundaries and in few areas within the landslide body. As expected, the results provided by Cosmo-SkyMed are more detailed

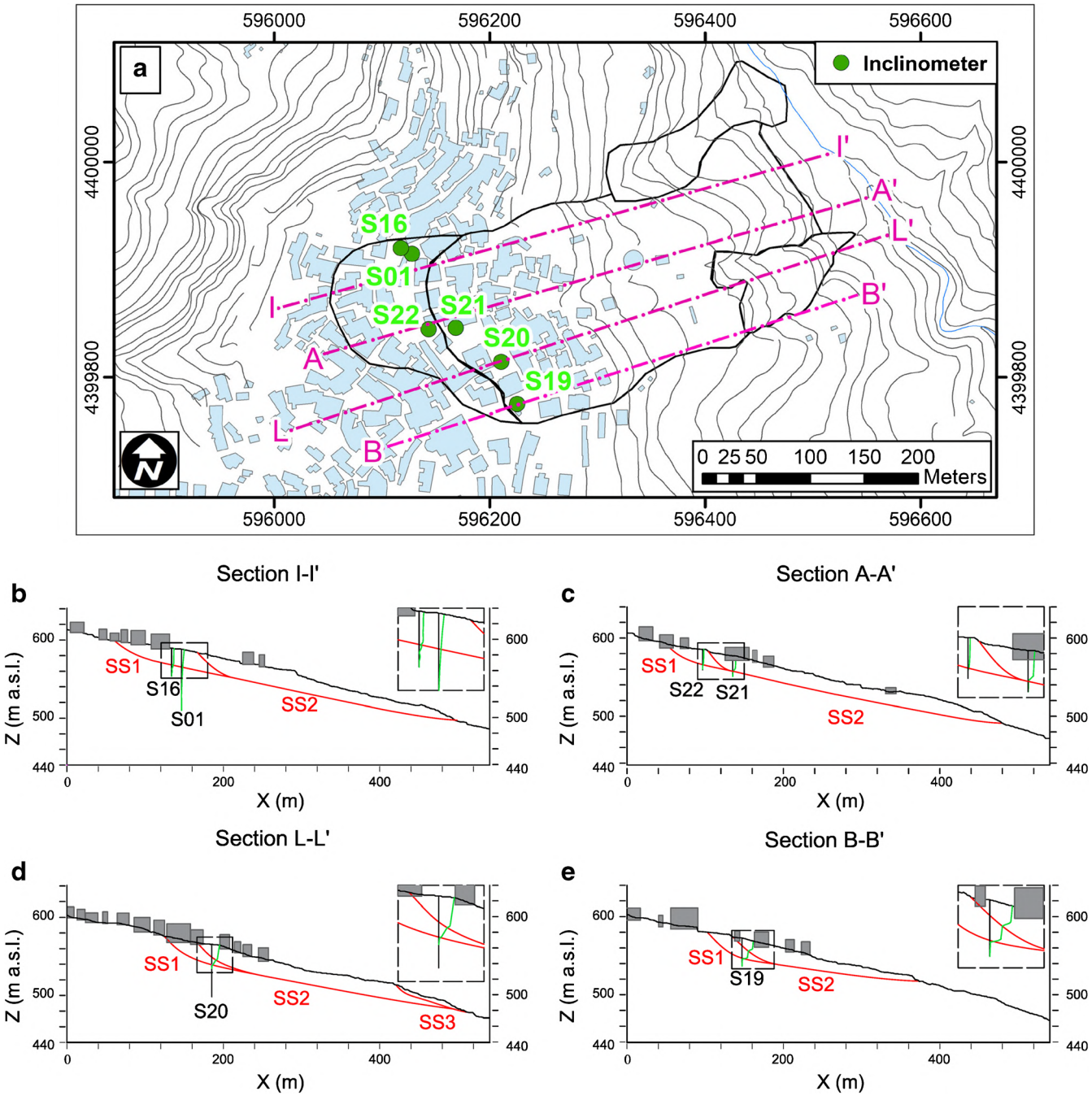

Fig. 8 Kinematic model of the landslide: (**a**) traces of the longitudinal cross sections; (**b**-**e**) reconstructed cross-sections of the landslide (i.e. kinematic model) with indication of the detected sliding surfaces (SS1 and SS2) from inclinometers

(thanks to the higher ground resolution of this system), thus allowing an improved zoning of areas with different velocity values.

Moreover, the eastern landslide body exhibits higher velocity values than the western one. Accordingly, as an improvement of the landslide analysis carried out by Gullà et al. (2017), the kinematic model and the interpretation of the *DGV maps* allowed typifying the landslide into two different bodies T_D1 and T_D2 (Fig. 10e). Particularly, for T_D1, the average velocity values recorded by all Envisat PSs (period 2003-2010) and CSK PSs (period 2012-2014) are both equal to approximately to 10 mm/year. As for T_D2, the average PS velocity values recorded are approximately equal to 16 mm/year during both considered periods. It is noteworthy that this discrepancy in velocity between T_D1 and T_D2 is also confirmed by the point-wise information provided by the inclinometers that show an average velocity equal to 3.2 mm/year for T_D1 (including S01, S16, S22) and 10.4 mm/year for T_D2 (including S19, S20, S21) over the period 2006–2014.

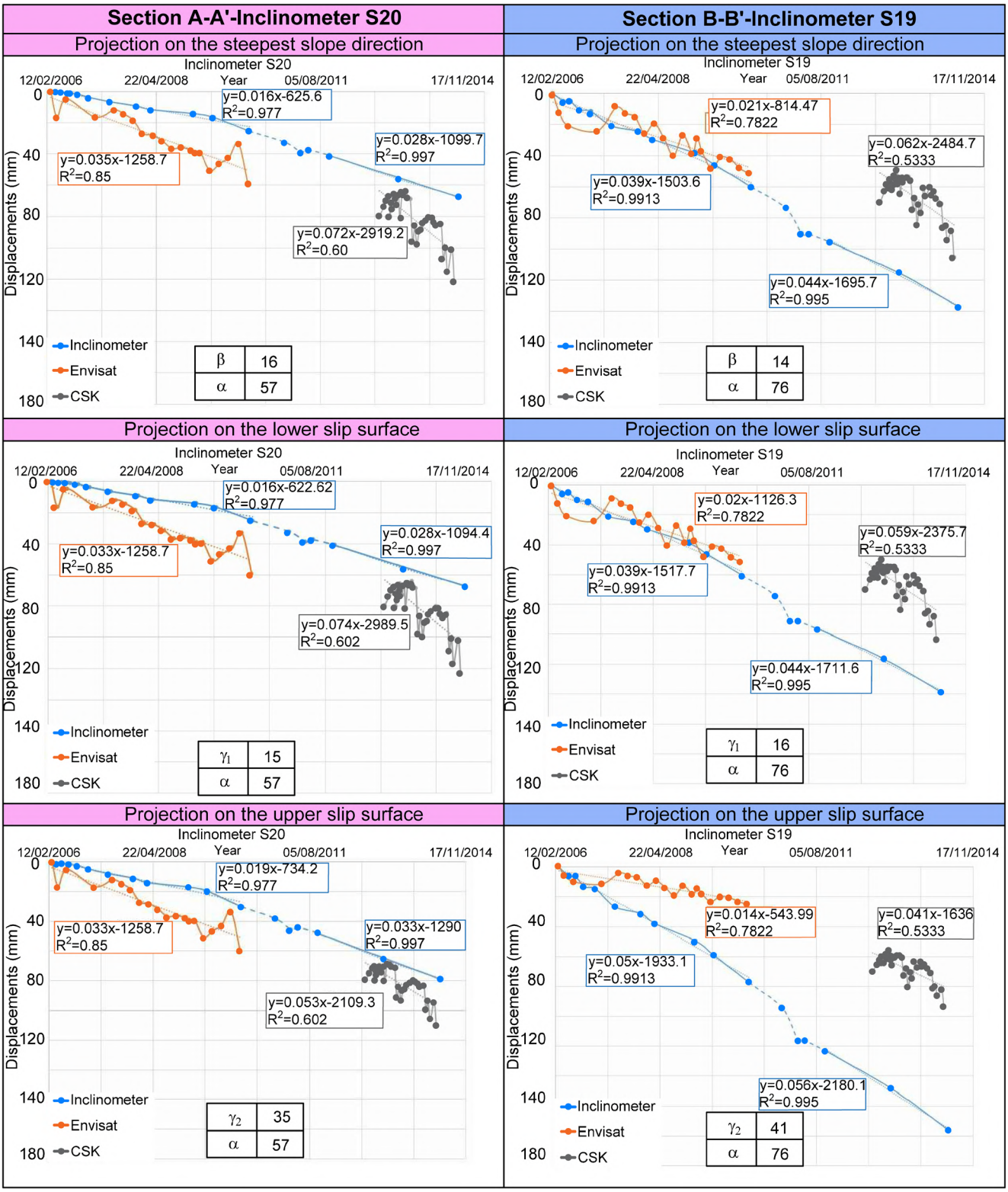

Fig. 9 Example of the comparison of A-DInSAR data with measurements from S19 and S20 inclinometers based on three different kinematic types

Table 2 Summary of the comparison between inclinometric and A-DInSAR (both Envisat and CSK) velocity (V) taking into account the position of the inclinometer with respect to the sliding surfaces of the landslide (see the cross-sections in Fig. 8b–e) and the direction assumed for the projection

Projection direction	Steepest Slope Direction						Lower Slip Surface			
Period	2003–2010			2012–2014			2003–2010			2012-2014
Incl.	$V_{Incl.}$	$V_{ENV.}$	ΔV	$V_{Incl.}$	V_{CSK}	ΔV	$V_{Incl.}$	$V_{ENV.}$	ΔV	$V_{Incl.}$
	[mm/year]	[mm/year]	[mm/year]	[mm/year]	[mm/year]	[mm/year]	[mm/year]	[mm/year]	[mm/year]	[mm/year]
S01	5.48	9.49	4.02	2.56	1.83	0.73	5.48	10.22	4.75	2.19
S16	3.39	5.11	1.71	2.85	1.82	1.02	2.85	4.38	1.53	2.52
S19	14.24	7.66	6.57	16.06	22.63	6.53	14.24	7.37	6.86	16.06
S20	6.21	11.89	5.69	10.22	26.43	16.21	6.21	11.83	5.62	10.22
S21	4.38	10.58	6.20	6.94	20.07	13.14	4.38	13.14	8.76	6.94
S22	1.83	5.48	3.65	1.83	9.49	7.66	1.83	6.25	4.38	1.83

Projection direction	Lower Slip Surface		Upper Slip Surface					
Period	2012-2014		2003–2010			2012–2014		
Incl.	V_{CSK}	ΔV	$V_{Incl.}$	$V_{ENV.}$	ΔV	$V_{Incl.}$	V_{CSK}	ΔV
	[mm/year]	[mm/year]	[mm/year]	[mm/year]	[mm/year]	[mm/year]	[mm/year]	[mm/year]
S01	1.83	0.36	-	-	-	-	-	-
S16	2.55	0.03	-	-	-	-	-	-
S19	21.17	5.11	14.60	5.14	9.45	15.70	15.00	0.69
S20	27.04	16.83	6.21	12.70	6.49	9.86	19.35	9.49
S21	19.71	12.77	-	-	-			
S22	8.39	6.56	-	-	-			

Inclinometric velocity is computed within the overlap period with Envisat (2003–2010) and CSK (2012-2014) data. Incl. stands for inclinometer; ENV. Stands for Envisat

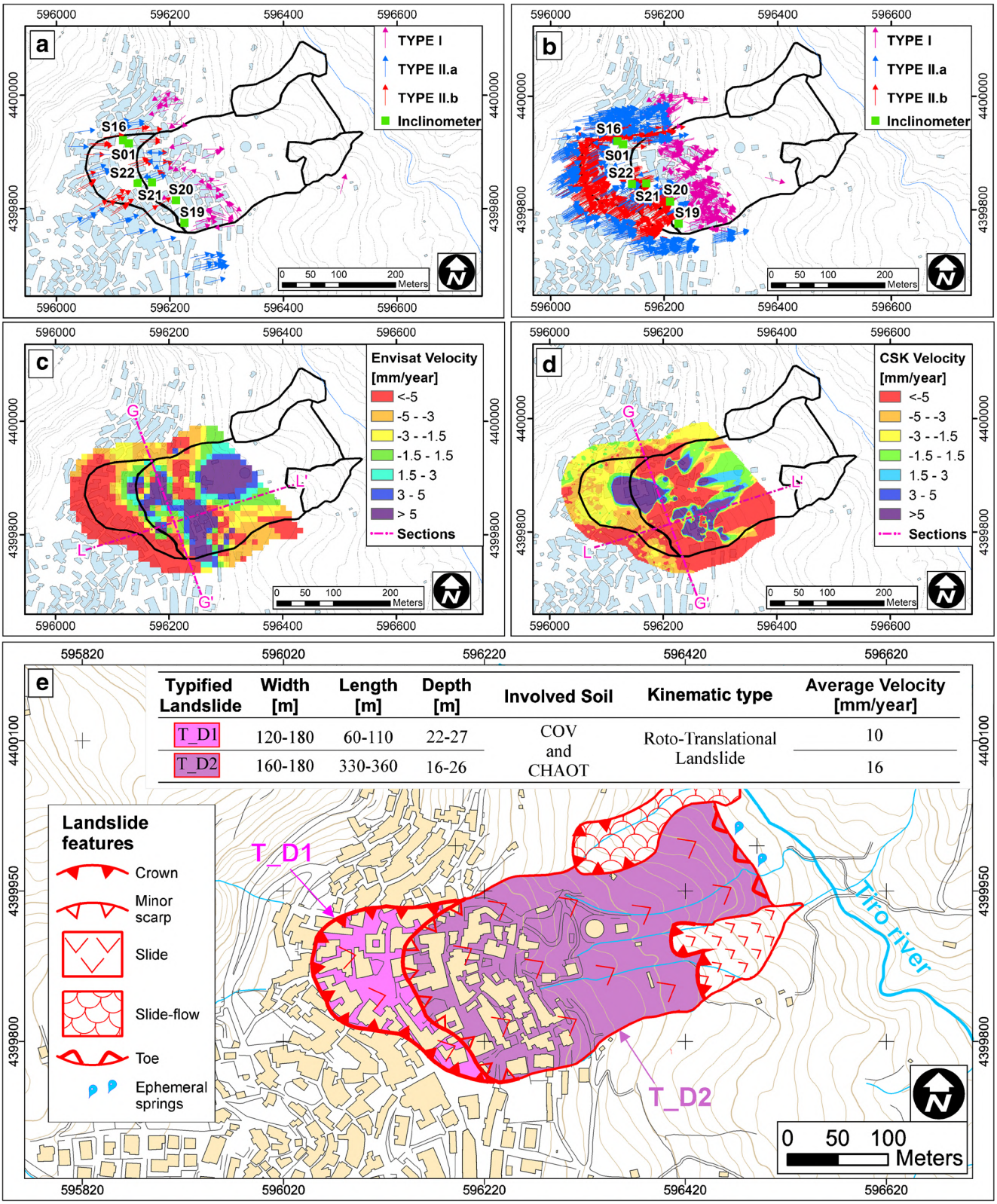

Fig. 10 Kinematic types used for the projection of (**a**) Envisat and (**b**) Cosmo-SkyMed data (arrows represent velocity vectors; the colours allows distinguishing the type of projection used); (**c**) *DGV map* based on Envisat data; (**d**) *DGV map* based on Cosmo-SkyMed data; (**e**) map of the typified landslide

Phase Ib: Building damage and their position

The purpose of Phase Ib was shedding a light on the role played by the position of the buildings within the landslide on both the damage occurrence and the severity level. To this aim, the available map of damaged buildings (Peduto et al. 2017b, 2018b) was analyzed with respect to six sections crossing the landslide area used to represent its kinematic model (Fig. 11a). In particular, three longitudinal (Figs. 11c, d and e) and three transverse (Figs. 11f, g and h) sections were analyzed; these latter were selected in order to involve as many buildings as possible. Buildings were distinguished as being located on either the head, or the main body, or the boundaries of the landslide. The graph in Fig. 11b shows a summary for the 65 analyzed buildings. It can be observed that (i) the buildings with Do to D1 damage level mainly concentrate in the landslide main body and they never occur in the landslide head, (ii) the percentage of D2 and D3 buildings in the main body is comparable with the sum of those in the head and on the boundaries and (iii) the number of buildings exhibiting D4 to D5

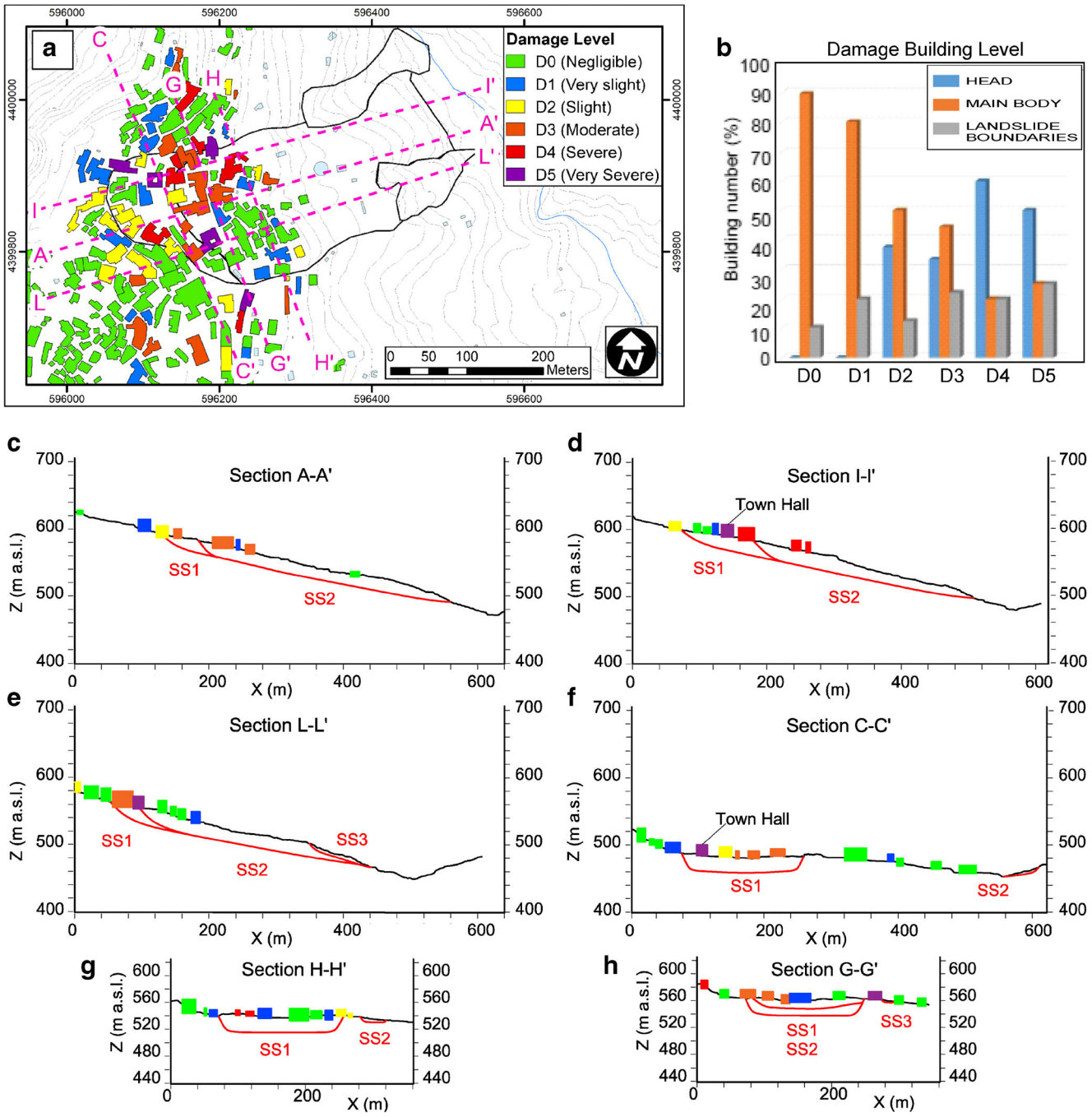

Fig. 11 **a** Distribution map of damage to buildings. **b** Percentage of buildings located in different landslide zones distinguished according their damage severity level. **c–h** Cross sections of the landslide with damaged buildings

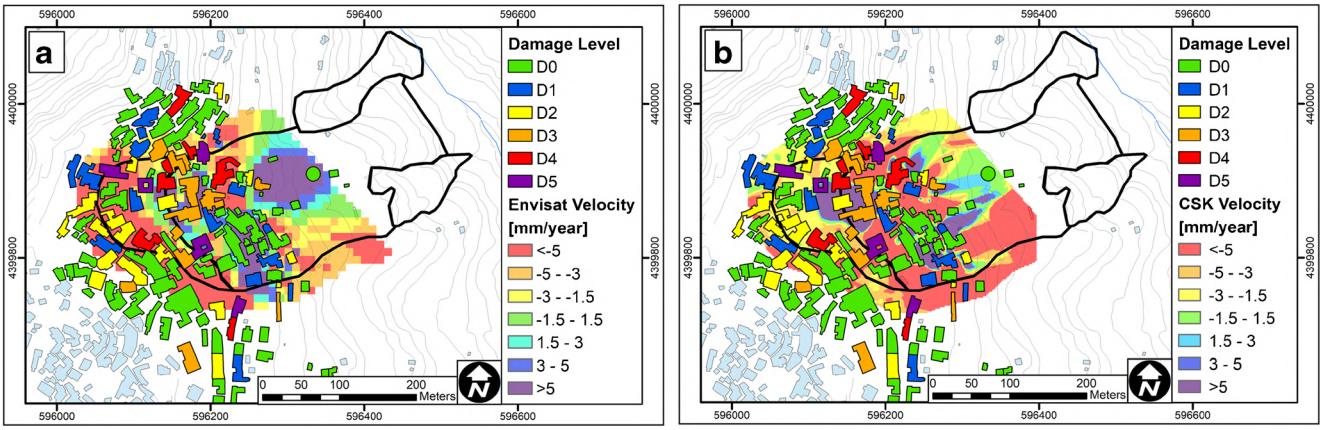

Fig. 12 *A-DInSAR-geotechnical velocity* (DGV) map vs. building damage map: (**a**) Envisat (2003–2010) data; (**b**) Cosmo-SkyMed (2012–2014) data

damage levels is higher in the landslide heads than in the main body or along the boundaries (see also Ciampalini et al. 2014).

Phase II: Damage distribution and kinematic aspects

The aim of this stage was to identify possible relationships between the detailed velocity field of the phenomenon and both the distribution and the severity of the damage. Thus, a comparison was made between the map of damage severity distribution and the *DGV maps* relevant to both Envisat (Fig. 12a) and Cosmo-SkyMed (Fig. 12b) data. Both Figures show that buildings with highest damage severity levels concentrate in the head and along the boundaries of the landslide; herein the highest velocity values (and their gradients) are recorded. However, some buildings with D3-D5 damage levels are present within the landslide body in correspondence of local "anomalous" higher velocity values.

Discussion

The results show that beside the fact that A-DInSAR data can provide an overview of the kinematics of the landslides—as already pointed out by several Authors (among others, Cascini et al. 2010, 2013; Frattini et al. 2018; Gullà et al. 2017; Wasowski and Pisano 2019)—their full integration with ground-based geotechnical monitoring data allows deriving the *DGV map* capable of spreading the detailed kinematic information (deriving from inclinometers) within the boundaries of the landslide at hand. With reference to inclinometric data, although two inclinometers (So1 and S22) measured extremely slow displacement velocity values that are below the typical precision of inclinometers (Mikkelsen 2003; Refice et al. 2019; Stark and Choi 2008; Wasowski and Pisano 2019), they were all considered in the analyses (similar cases in literature are provided by Corsini et al. 2005; Tommasi et al. 2006; Calcaterra et al. 2010) taking into account the extremely accurate measurement procedure adopted in the specific case and the overall agreement with both A-DInSAR data analysis and geomorphological landslide features. However, further checks on these two inclinometers will be carried out.

To investigate further the link between building damage and the geometry-kinematics of the landslide phenomenon, one longitudinal and one transverse cross-sections were considered. For these sections, the damage level of the buildings and their position on the landslide profile as well as the velocity along a selected section were correlated. These operations were carried out both for Envisat (Fig. 13a and b) and for Cosmo-SkyMed data (Fig. 13c and d). The longitudinal section L-L' shows that damaged buildings concentrate between the head of T_D1 and the scarp of T_D2. Furthermore, the velocity trend along the section shows an alternation of negative (downward along the slip surface or downslope along the steepest slope direction, depending on the Type of projection adopted in the specific location) and positive (upward along the slip surface or upslope along the steepest slope direction, depending on the Type of projection adopted in the specific location) values of projected velocity moduli in correspondence of some sectors of the landslide that can be associated with the effects of localized rotational movements. The G-G' cross-section shows an alternation of negative (downslope/downward) and positive (upslope/upward) values of projected velocity moduli in correspondence of the landslide boundaries due to the presence of a rotational component. Furthermore, the damage distribution for section G-G' confirms that the most severe damage is recorded along (or in proximity of) the landslide boundaries.

The comparison between the damage distribution and the *DGV maps* shows that the buildings—of masonry type with shallow foundations—located in the landslide-affected area exhibit higher damage severity levels in correspondence of the head, the secondary scarp and the boundaries of the landslide where the highest velocity gradients are recorded and the highest differential settlements may affect buildings located therein (Nicodemo et al. 2017b). However, some local anomalies (i.e. areas with high velocity values within the landslide body) seem to provide an apparent mismatch with the overall kinematics of the phenomenon. For this reason, a more in-depth analysis of the phenomenon was necessary. Knowing that both the geology and soil mechanical properties, although chaotic, are uniformly distributed within the landslide, the presence of any possible local conditioning factors such as sub-services that could interfere with the landslide was analyzed. This investigation revealed the presence of some buried channels collecting the runoff water together with the water captured by a drainage tunnel built uphill (Fig. 14). From the comparison of the Cosmo-SkyMed *DGV map* (Fig. 14a) with the tracks

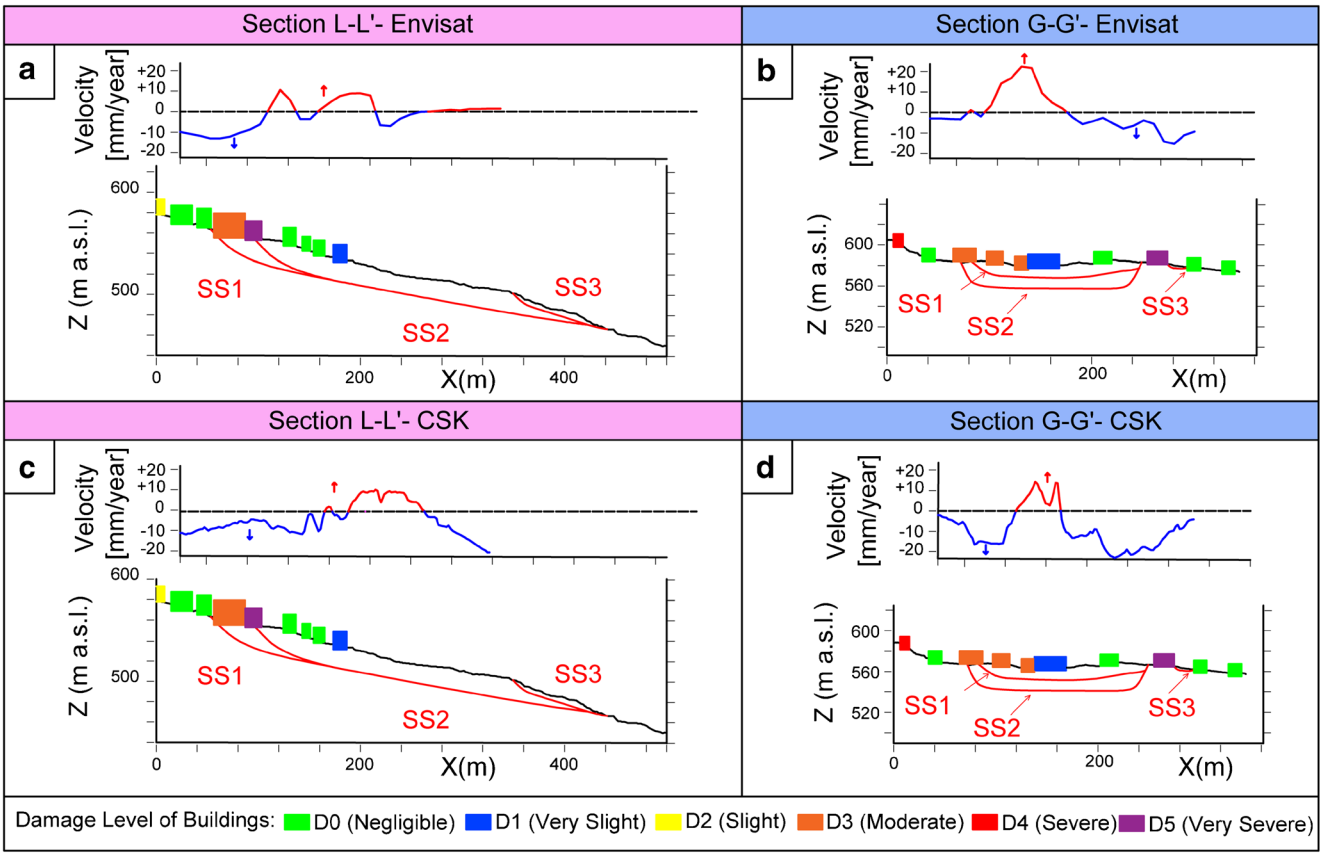

Fig. 13 Comparison between the damage severity of the buildings and Envisat/Cosmo-SkyMed velocity from DGV map in sections L-L′ (**a** and **c**) and G-G′ (**b** and **d**)

of the channels, it seems that the zones with local changes in velocities inside the landslide body are in correspondence of the channels. Furthermore, it also seems that the damage level is higher for buildings close to the channels (Fig. 14b). Indeed, these latter may have been damaged by the landslide displacements in time and the point-wise water losses may have caused the localized velocity increase and the associated "anomalous" damage severity.

Conclusions

The present work tried to provide a further contribution to the studies previously carried out in the urban centre of Lungro passing from the municipal scale (Gullà et al. 2017; Peduto et al. 2017b, 2018b) to the scale of the single slope. In particular, as a key step forward, innovative non-invasive spaceborne A-DInSAR data and the results of geotechnical characterization and conventional monitoring—providing information on landslide displacements, position of slip surfaces with reference to the characteristics of the involved geomaterials—were integrated with the results of building damage surveys in order to detail the kinematic characteristics of a landslide affecting the historic centre as well as to address further analyses aimed at clarifying the role of buried services on both the landslide and the exposed buildings.

The analysis allowed outlining the instability phenomenon affecting the historic centre of Lungro as consisting of a slow-moving landslide with two translational sliding bodies with slight rotational character immediately downstream of the two escarpment sectors. The inclinometers revealed the presence of a medium-deep sliding surface at depths ranging between 18 and 27 m mainly involving the relatively finer grain fraction of COV and CHAOT geomaterials. As a step forward with respect to previous studies, the landslide was typified in two different bodies T_D1 and T_D2 exhibiting average velocity of 10 mm/year and 16 mm/year, respectively. This goal was achieved by using the novel advanced *DGV maps*—providing the end-user with a 3D velocity vector map—that fully exploit the capability of remote sensing data for landslide kinematic characterization at the slope scale, especially when corroborated by the interpretation of geotechnical data dealing with soil properties (identification of weak bands involving fine-grained soils) and inclinometric measurements.

The followed approach allowed (i) distinguishing portions of the landslide that exhibit either mainly rotational or translational displacements, (ii) checking the distribution of building damage severity with respect to the kinematic features of the landslide and (iii) associating both localized anomalous velocity values and damage with the presence of underground services.

The level of knowledge acquired on the landslide in the present study can be used immediately to manage landslide risk in the short term and is propaedeutic to set up and calibrate an advanced coupled geotechnical-structural model to simulate the landslide displacements and the building performance over medium/long period and, therefore, to set up appropriate risk mitigation strategies. These latter, taking advantage of the identification of the "cause" of the anomalous high velocity/damage locations, may address the risk mitigation by planning interventions pursuing the reduction of either the "cause"—by

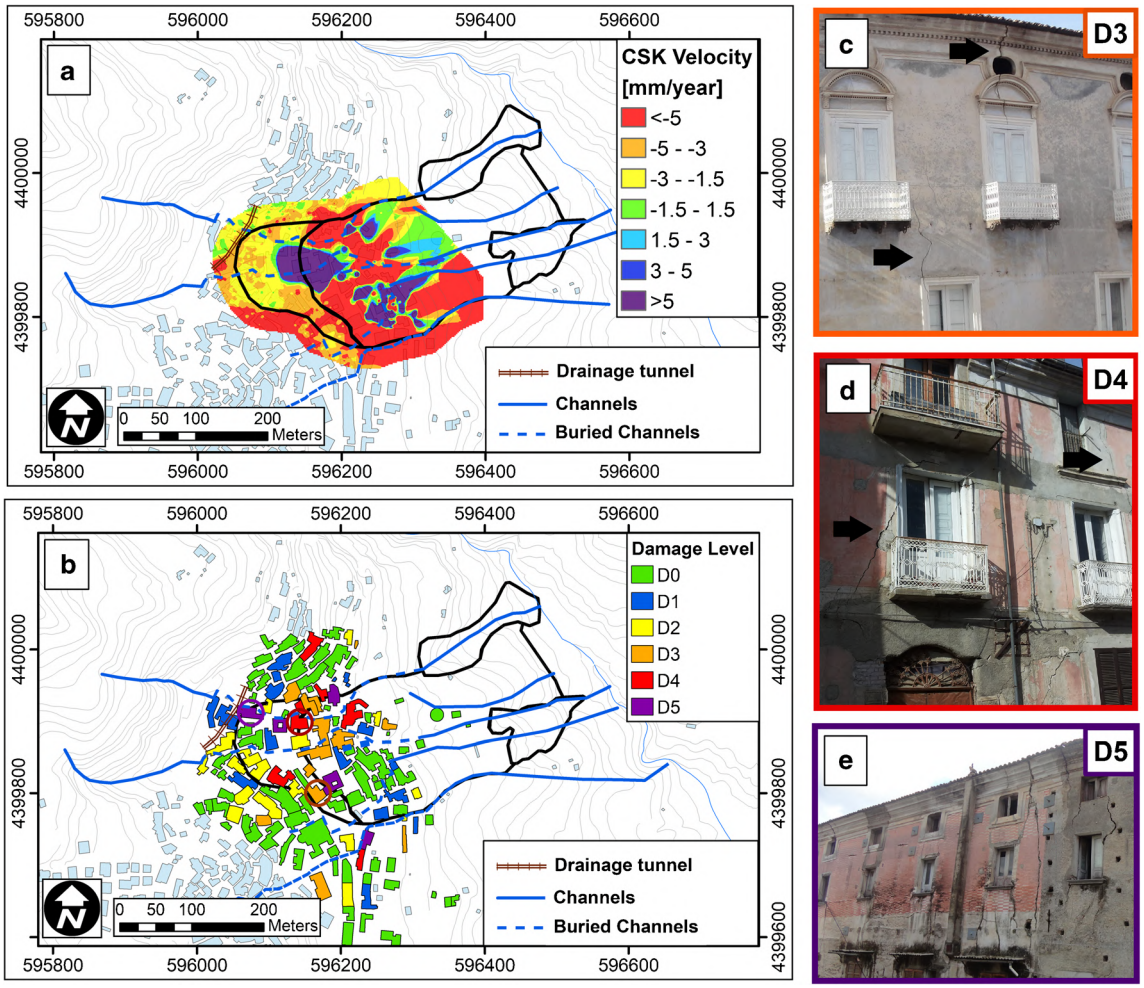

Fig. 14 Possible conditioning factors of slope instability: (**a**) paths of the buried channels vs. Cosmo-SkyMed velocity; (**b**) paths of the buried channels vs. the damage severity level of the buildings; photos of damaged buildings (labelled with coloured circles in Fig. 14b) in proximity of buried channels with indication of damage level: (**c**) D3; (**d**) D4; (**e**) D5

maintenance works to the buried channels—or the vulnerability of the buildings by increasing the "structural strength" of the building and/or of the foundation system.

Acknowledgements

The work was partially funded by the Agreement for Research contribution signed between Italian National Research Council (CNR-IRPI) and the Department of Civil Engineering of the University of Salerno (responsible persons: Giovanni Gullà—CNR-IRPI and Dario Peduto—University of Salerno) on the topic: "*Analisi quantitativa del rischio da frane a cinematica lenta in aree urbane dell'Appennino Meridionale con l'ausilio di modellazione numerica avanzata e dati di monitoraggio satellitare*". This work is also part of the Progetto DTA.AD003.077 "*Tipizzazione di eventi di dissesto idrogeologico*" of the CNR—Department of "Scienze del sistema Terra e Tecnologie per l'Ambiente".

The work is also framed within the activity of the ICL-IPL project No 248: *Innovation in slow-moving landslide risk assessment of roads and urban sites by combining multi-sensor multi-source monitoring data*.

The Authors are grateful to Gianfranco Fornaro and Diego Reale from IREA-CNR, Naples for A-DInSAR data processing.

The Authors wish to thank the Editor and two anonymous Reviewers who helped to improve the paper in its final version with their valuable suggestions.

Funding Open access funding provided by Università degli Studi di Salerno within the CRUI-CARE Agreement.

References

Abolmasov B, Milenkovic S, Jelisavac B, Radic Z (2015) The analysis of landslide dynamics based on automated GNSS monitoring—a case study. Engi Geol Soc Territory Landslide Processes 2:143–146

Antronico L, Petrucci O, Sorriso-Valvo M (1996) I fenomeni franosi nella tavoletta "Montalto Uffugo" (CS) risultati inattesi dall'analisi delle relazioni tra morfometria e tipologia delle frane e litologia dei versanti. Geol Appl Idrogeol 31(4):187–201

Antronico L, Borrelli L, Coscarelli R, Gullà G (2015) Time evolution of landslide damages to buildings: the case study of Lungro (Calabria, southern Italy). Bull Eng Geol Environ 74(1):47–59

Antronico L, Borrelli L, Peduto D, Fornaro G, Gullà G, Paglia L, Zeni G (2013) Conventional and innovative techniques for the monitoring of displacements in landslide affected area. Landslide science and practice. Springer, Berlin, pp 125–131

Auflič JM, Mikoš M, Verbovšek T, Arbanas Ž, Mihalić Arbanas S (2018) 3rd Regional Symposium on Landslides in the Adriatic-Balkan Region (3rd ReSyLAB)—a final report (Conference Paper). Landslides 15(2):381–384

Bianchini S, Cigna F, Righini G, Proietti C, Casagli N (2012) Landslide hotspot mapping by means of persistent scatterer interferometry. Environ Earth Sci 67:1155–1172

Bianchini S, Ciampalini A, Raspini F, Bardi F, Di Traglia F, Moretti S, Casagli N (2014) Multi-temporal evaluation of landslide movements and impacts on buildings in San Fratello (Italy) by means of C-band and X-band PSI data. Pure Appl Geophys 172(11):3043–3065

Bianchini S, Pratesi F, Nolesini T, Casagli N (2015) Building deformation assessment by means of persistent scatterer interferometry analysis on a landslide-affected area: the Volterra (Italy) case study. Remote Sens 7(4):4678–4701

Borrelli L, Ciurleo M, Gullà G (2018) Shallow landslide susceptibility assessment in granitic rocks using GIS-based statistical methods: the contribution of the weathering grade map. Landslides 15(6):1127–1142

Borrelli L, Gullà G (2017) Tectonic constraints on a deep-seated rock slide in weathered crystalline rocks. Geomorphology 290:288–316

Burland JB, Broms BB, de Mello VFB (1977) Behaviour of foundations and structures. In: SOA Report, Proc of the 9th Int Conf on Soil Mechanics and Foundation Engineering, vol 2, Tokyo, pp 495–546

Calcaterra S, Cesi C, Di Maio C, Gambino P, Merli K, Vallario M, Vassallo R (2010) Surface displacements of two landslides evaluated by GPS and inclinometer systems: a case study in Southern Apennines, Italy. Nat Hazards. https://doi.org/10.1007/s11069-010-9633-3

Calò F, Ardizzone F, Castaldo R, Lollino P, Tizzani P, Guzzetti F, Manunta M (2014) Enhanced landslide investigations through advanced DInSAR techniques: The Ivancich case study, Assisi, Italy. Remote Sens Environ 142:69–82

Casagli N, Frodella W, Morelli S, Tofani V, Ciampalini A, Intrieri E, Raspini F, Rossi G, Tanteri L, Lu P (2017) Spaceborne, UAV and ground-based remote sensing techniques for landslide mapping, monitoring and early warning. Geoenviron Disast 4(1):9

Cascini L, Fornaro G, Peduto D (2009) Analysis at medium scale of low-resolution DInSAR data in slow-moving landslide-affected areas. ISPRS J Photogramm Remote Sens 64(6):598–611

Cascini L, Fornaro G, Peduto D (2010) Advanced low-and full-resolution DInSAR map generation for slow-moving landslide analysis at different scales. Eng Geol 112(1-4):29–42

Cascini L, Gullà G, Sorbino G (2006) Groundwater modelling of a weathered gneissic cover. Can Geotech J 43:1153–1166

Cascini L, Peduto D, Pisciotta G, Arena L, Ferlisi S, Fornaro G (2013) The combination of DInSAR and facility damage data for the updating of slow-moving landslide inventory maps at medium scale. Nat Hazards Earth Syst Sci 13(6):1527

Castaldo R, Tizzani P, Calò F, Ardizzone F, Lanari R, Guzzetti F, Manunta M (2015) Landslide kinematical analysis through inverse numerical modelling and differential SAR interferometry. Pure Appl Geophys 172:3067–3080. https://doi.org/10.1007/s00024-014-1008-3

Ciampalini A, Bardi F, Bianchini S, Frodella W, Del Ventisette C, Moretti S, Casagli N (2014) Analysis of building deformation in landslide area using multisensor PSInSAR™ technique. Int J Appl Earth Obs Geoinf 33:166–180

Cigna F, Lasaponara R, Masini N, Milillo P, Tapete D (2014) Persistent scatterer interferometry processing of COSMO-SkyMed StripMap HIMAGE time series to depict deformation of the historic centre of Rome, Italy. Remote Sens 6(12):12593–12618

Colesanti C, Wasowski J (2006) Investigating landslides with space-borne Synthetic Aperture Radar (SAR) interferometry. Eng Geol 88(3-4):173–199

Corominas J, Van Westen C, Frattini P, Cascini L, Malet JP, Fotopoulou S, Catani F, Van Den Eechaut M, Mavrouili O, Agliardi F, Pitilakis K, Winter MG, Pastor M, Ferlisi S, Tofani V, Hervas J, Smith JT (2014) Recommendations for the quantitative analysis of landslide risk. Bull Eng Geol Environ 73(2):209–263

Corsini A, Pasuto A, Soldati M (2005) Zannonib A (2005) -Field monitoring of the Corvara landslide (Dolomites, Italy) and its relevance for hazard assessment. Geomorphology 66:149–165

Cotecchia F, Lollino P, Petti R (2016) Efficacy of drainage trenches to stabilise deep slow landslides in clay slopes. Géotechnique Lett 6(1):1–6

Crosetto M, Gili JA, Monserrat O, Cuevas-González M, Corominas J, Serral D (2013) Interferometric SAR monitoring of the Vallcebre landslide (Spain) using corner reflectors. Nat Hazards Earth Syst Sci 13(4):923–933

Crosetto M, Monserrat O, Cuevas-González M, Devanthéry N, Crippa B (2016) Persistent scatterer interferometry: a review. IPRS J Photogramm Remote Sens 115:78–89

Crosetto M, Copons R, Cuevas-González M, Devanthéry N, Monserrat O (2018) Monitoring soil creep landsliding in an urban area using persistent scatterer interferometry (El Papiol, Catalonia, Spain). Landslides 15(7):1317–1329

Cruden DM, Varnes DJ (1996) Landslide types and processes. In: Turner AK, Schuster RL (eds) Landslides investigation and mitigation. Transportation research board, US National Research Council, Washington DC, Special Report 247, Chapter 3, pp 36–75

Del Soldato M, Riquelme A, Bianchini S, Tomàs R, Di Martire D, De Vita P, Moretti S, Calcaterra D (2018) Multisource data integration to investigate one century of evolution for the Agnone landslide (Molise, southern Italy). Landslides 15:2113–2128

Del Soldato M, Solari L, Poggi F, Raspini F, Tomás R, Fanti R, Casagli N (2019) Landslide-induced damage probability estimation coupling InSAR and field survey data by fragility curves. Remote Sens 11:1486. https://doi.org/10.3390/rs11121486

Di Maio C, Fornaro G, Gioia D, Reale D, Schiattarella M, Vassallo R (2018) In situ and satellite long-term monitoring of the Latronico landslide, Italy: Displacement evolution, damage to buildings, and effectiveness of remedial works. Eng Geol 245:218–235

Fell R, Corominas J, Bonnard C, Cascini L, Leroi E, Savage WZ (2008) Guidelines for landslide susceptibility, hazard and risk zoning for land-use planning. Eng Geol 102(3-4):99–111

Ferlisi S, Peduto D, Gullà G, Nicodemo G, Borrelli L, Fornaro G (2015) The use of DInSAR data for the analysis of building damage induced by slow-moving landslides. In: Engineering Geology for Society and Territory, vol 2. Springer, Cham, pp 1835–1839

Ferlisi S, Gullà G, Nicodemo G, Peduto D (2019) A multi-scale methodological approach for slow-moving landslide risk mitigation in urban areas, southern Italy. Euro-Mediterr J Environ Integr. https://doi.org/10.1007/s41207-019-0110-4

Fornaro G, Pauciullo A, Serafino F (2009) Deformation monitoring over large areas with multipass differential SAR interferometry: A new approach based on the use of spatial differences. Int J Remote Sens 30(6):1455–1478

Fornaro G, Verde S, Reale D, Pauciullo A (2014) CAESAR: An approach based on covariance matrix decomposition to improve multibaseline–multitemporal interferometric SAR processing. IEEE Trans Geosci Remote Sens 53(4):2050–2065

Frattini P, Crosta GB, Allievi J (2013) Damage to buildings in large slope rock instabilities monitored with the PSInSAR™ technique. Remote Sens 5(10):4753–4773. https://doi.org/10.3390/rs5104753

Frattini P, Crosta GB, Rossini M, Allievi J (2018) Activity and kinematic behaviour of deep-seated landslides from PS-InSAR displacement rate measurements. Landslides 15(6):1053–1070

Greco R, Sorriso-Valvo M, Catalano E (2007) Logistic regression analysis in mass movement susceptibility: the Aspromonte case study, Calabria, Italy. Eng Geol 89(1–12):47–66

Guzzetti F, Mondini AC, Cardinali M, Fiorucci F, Santangelo M, Chang KT (2012) Landslide inventory maps: new tools for and old problem. Earth-Sci Rev 112:42–66

Guerricchio A, Doglioni A, Simeone V (2012) Tectonic-gravitational deep-seated failures and macro-landslides in Scilla and Punta Pezzo area (Southern Calabria - Italy). Rend Online Soc Geol Ital 21(1):367–369

Gullà G, Peduto D, Borrelli L, Antronico L, Fornaro G (2017) Geometric and kinematic characterization of landslides affecting urban areas: the Lungro case study (Calabria, Southern Italy). Landslides 14(1):171–188

Hanssen RF (2001) Radar Interferometry: Data Interpretation and Error Analysis, vol 2. Springer-Verlag, Berlin

Herrera G, Fernandez-Merodo J, Tomas R, Cooksley G, Mulas J (2009) Advanced interpretation of subsidence in Murcia (SE Spain) using A-DInSAR data-modelling and validation. Nat Hazards Earth Syst Sci 9:647–661

Herrera G, Gutiérrez F, García-Davalillo JC, Guerrero J, Notti D, Galve JP, Fernàndez-Merodo JA, Cooksley G (2013) Multi-sensor advanced DInSAR monitoring of very slow landslides: the Tena Valley case study (Central Spanish Pyrenees). Remote Sens Environ 128:31–43

Hilley GE, Burgbman R, Ferretti A, Novali F, Rocca F (2004) Dynamics of slow moving landslides from Permanent Scatterer Analysis. Science 304(5679):1952–1955

Iannace A, Bonardi G, D'Errico M, Mazzoli S, Perrone V, Vitale S (2005) Structural setting and tectonic evolution of the Apennine Units of northern Calabria. Compt Rendus Geosci 337(16):1541–1550

Infante D, Di Martire D, Confuorto P, Tessitore S, Ramondini M, Calcaterra D (2018). Differential SAR interferometry technique for control of linear infrastructures affected by ground instability phenomena. International Archives of the Photogrammetry, Remote Sensing and Spatial Information Sciences, 42(3/W4)

Jaboyedoff M, Del Gaudio V, Derron MH, Grandjean G, Jongmans D (2019) Characterizing and monitoring landslide processes using remote sensing and geophysics. Eng Geol 259:105167

Lu P, Catani F, Tofani V, Casagli N (2014) Quantitative hazard and risk assessment for slow-moving landslides from Persistent Scatterer Interferometry. Landslides 11(4):685–696

Mikkelsen PE (2003) Advances in Inclinometer Data Analysis. Proceedings of the 6th International Symposium on Field Measurements in Geomechanics, Oslo, Norway, 15-18 September 2003; Myrvoll, F. Ed.; A.A. Balkema, Lisse, Abingdon; pp. 555-566

Merodo JAF, Davalillo JCG, Herrera G, Mira P, Pastor M (2014) 2D viscoplastic finite element modelling of slow landslides: the Portalet case study (Spain). Landslides 11:29–42

Nappo N, Peduto D, Mavrouli O, van Westen CJ, Gullà G (2019) Eng Geol 260 (2019), https://doi.org/10.1016/j.enggeo.2019.105244

Nicodemo G, Ferlisi S, Peduto D, Aceto L, Gullà G (2020). Damage to masonry buildings interacting with slow-moving landslides: a numerical analysis, Lecture Notes in Civil Engineering, F. Calvetti et al. (Eds.): CNRIG 2019, LNCE 40, pp. 52–61, 2020, © Springer Nature Switzerland AG 2020, https://doi.org/10.1007/978-3-030-21359-6_6

Nicodemo G, Peduto D, Ferlisi S, Gullà G, Borrelli L, Fornaro G, Reale D (2017a). Analysis of building vulnerability to slow-moving landslides via A-DInSAR and damage survey data. In M. Mikos et al. (eds.), Advancing Culture of Living with Landslides, Proc. Of 4th World Landslide Forum, Ljubljana, 30 maggio – 2 giugno 2017, © Springer International Publishing AG 2017, vol.2, set 2, pp. 899-907, https://doi.org/10.1007/978-3-319-53498-5_102, ISBN: 978-3-319-53497-8.

Nicodemo G, Peduto D, Ferlisi S, Gullà G, Reale D, Fornaro G (2018). DINSAR data integration in vulnerability analyses of buildings exposed to slow-moving landslides. Proc. Of IEEE International Geoscience and Remote Sensing Symposium (IGARSS 2018), Valencia, Spain, July 22-27, 2018, pp. 6111-6114, https://doi.org/10.1109/IGARSS.2018.8518808, ISBN: 978-1-5386-7150-4. https://ieeexplore.ieee.org/document/8518808

Nicodemo G, Peduto D, Ferlisi S, Maccabiani J (2017b) Investigating building settlements via very high resolution SAR sensors. In: Bakker, Frangopol, van Breugel (eds) Life-Cycle of Engineering Systems: Emphasis on Sustainable Civil Infrastructure. Taylor & Francis Group, London, pp 2256–2263 ISBN 978-1-138-02847-0

North M, Farewell T, Hallet S, Bertelle A (2017) Monitoring the response of roads and railways to seasonal soil movement with Persistent Scatterers Interferometry over six UK sites. Remote Sens 9:1–17

Palmisano F, Vitone C, & Cotecchia F (2016). Landslide damage assessment at the intermediate to small scale. In Landslides and engineered slopes. Experience, theory and practice. Proc of the 12th Int Symp on Landslides, CRC Press/Balkema, 3, pp. 1549-1557

Peduto D, Borrelli L, Antronico L, Gullà G, Fornaro G (2016) An integrated approach for landslide characterization in a historic centre. In: Aversa S, Cascini L, Picarelli L, Scavia C (eds) Landslides and engineered slopes. Experience, theory and practice. Proc of the 12th Int Symp on Landslides, vol 3. CRC Press, Balkema, pp 1575–1581. https://doi.org/10.1201/b21520-195

Peduto D, Cascini L, Arena L, Ferlisi S, Fornaro G, Reale D (2015) A general framework and related procedures for multiscale analyses of DInSAR data in subsiding urban areas. ISPRS J Photogramm Remote Sens 105:186–210 ISSN 0924-2716, https://doi.org/10.1016/j.isprsjprs.2015.04.001

Peduto D, Nicodemo G, Maccabiani J, Ferlisi S (2017a) Multi-scale analysis of settlement-induced building damage using damage surveys and DInSAR data: a case study in The Netherlands. Eng Geol 218:117–133

Peduto D, Elia F, Montuori R (2018a) Probabilistic analysis of settlement-induced damage to bridges in the city of Amsterdam (The Netherlands). Transport Geotech 14:169–182. https://doi.org/10.1016/j.trgeo.2018.01.002

Peduto D, Ferlisi S, Nicodemo G, Reale D, Pisciotta G, Gullà G (2017b) Empirical fragility and vulnerability curves for buildings exposed to slow-moving landslides at medium and large scales. Landslides 14(6):1993–2007

Peduto D, Korff M, Nicodemo G, Marchese A, Ferlisi S (2019a) Empirical fragility curves for settlement-affected buildings: analysis of different intensity parameters for seven hundred masonry buildings in The Netherlands. Soils Found 59(2):380–397. https://doi.org/10.1016/j.sandf.2018.12.009

Peduto D, Nicodemo G, Caraffa M, Gullà G (2018b) Quantitative analysis of consequences to masonry buildings interacting with slow-moving landslide mechanisms: a case study. Landslides 15(10):2017–2030

Peduto D, Nicodemo G, Cuevas-Gonzáles M, Crosetto M (2019b) Analysis of damage to buildings in urban centres on unstable slopes via TerraSAR-X PSI data: the case study of El Papiol town (Spain). IEEE Geosci Remote Sens Lett 16(11):1706–1710, Print ISSN: 1545-598X, Online ISSN: 1558-0571. https://doi.org/10.1109/LGRS.2019.2907557

Plank S, Singer J, Minet Ch, Thuro K (2010) GIS based suitability evaluation of the differential radar interferometry method (DInSAR) for detection and deformation monitoring of landslides, in: Proceedings of Fringe 2009 Workshop, edited by: Lacoste- Francis, H., 30 November–4 December 2009, ESRIN, Frascati, Italy (ESA SP-677), 8 pp., ISBN: 978-92-9221- 41-4, 2010.

Raspini F, Bardi F, Bianchini S, Ciampalini A, Del Ventisette C, Farina P, Ferrigno F, Solari L, Casagli N (2017) The contribution of satellite SAR-derived displacement measurements in landslide risk management practices. Nat Hazards 86:327–351. https://doi.org/10.1007/s11069-016-2691-4

Raspini F, Bianchini S, Ciampalini A, Del Soldato M, Solari L, Novali F, Del Conte S, Rucci A, Ferretti A, Casagli N (2018) Continuous, semi-automatic monitoring of ground deformation using Sentinel-1 satellites. Sci Rep 8(1):7253

Refice A, Spalluto L, Bovenga F, Fiore A, Miccoli MN, Muzzicato P, Nitti DO, Nutricato R, Pasquariello G (2019) Integration of persistent scatterer interferometry and ground data for landslide monitoring: the Pianello landslide (Bovino, Southern Italy). Landslides 16:447–468

Sorriso-Valvo M, Sylvester AG (1993) The relationship between geology and landforms along a coastal mountain front, northern Calabria, Italy. Earth Surf Process Landf 18(3):257–273

Stark TD, Choi H (2008) Slope inclinometers for landslides. Landslides 5:339–350. https://doi.org/10.1007/s10346-008-0126-3

Tofani V, Raspini F, Catani F, Casagli N (2013) Persistent Scatterer Interferometry (PSI) technique for landslide characterization and monitoring. Remote Sens 5(3):1045–1065

Tommasi P, Pellegrini P, Boldini D, Ribacchi R (2006) Influence of rainfall regime on hydraulic conditions and movement rates in the overconsolidated clayey slope of the Orvieto hill (central Italy). Can Geotech J 43:70–86

Varnes DJ (1978) Slope movement types and processes. In: Landslides analysis and control. National Research Council Special Report, vol 176, pp 11–33

Wasowski J, Bovenga F (2014) Investigating landslides and unstable slopes with satellite Multi Temporal Interferometry: current issues and future perspectives. Eng Geol 174:103–138

Wasowski J, Bovenga F, Nutricato R, Nitti DO, Chiaradia MT (2017) High resolution satellite multi-temporal interferometry for monitoring infrastructure instability hazards. Innov Infrastruc Solut 2(1):27

Wasowski J, Pisano L (2019) Long-term InSAR, borehole inclinometer, and rainfall records provide insight into the mechanism and activity patterns of an extremely slow urbanized landslide. Landslides 17:445–457. https://doi.org/10.1007/s10346-019-01276-7

Winter MG, Shearer B, Palmer D, Peeling D, Harmer C, Sharpe J (2016) The Economic Impact of Landslides and Floods on the Road Network. Procedia Eng 143:1425–1434

D. Peduto (✉) · **M. Santoro**
Department of Civil Engineering,
University of Salerno,
Via Giovanni Paolo II, 132, 84084, Salerno, Fisciano, Italy
Email: dpeduto@unisa.it

M. Santoro
e-mail: marsantoro@unisa.it

L. Aceto · **L. Borrelli** · **G. Gullà**
Research Institute for Geo-Hydrological Protection,
National Research Council of Italy,
Via Cavour n. 4/6, 87030, Rende (Cosenza), Italy

L. Aceto
e-mail: luigi.aceto@irpi.cnr.it

L. Borrelli
e-mail: luigi.borrelli@irpi.cnr.it

G. Gullà
e-mail: giovanni.gulla@irpi.cnr.it